# SCATTERING DISTRIBUTION OF LIGHT FROM THIN FILM ROUGH LAYERS & LAYER STACKS FOR a-Si:H SOLAR CELLS.



BY

TADESSE BERGA

A THESIS SUBMITTED TO
THE SCHOOL OF GRADUATE STUDIES
ADDIS ABABA UNIVERSITY

IN PARTIAL FULFILMENT OF
THE REQUIREMENT FOR DEGREE OF
MASTER OF SCIENCE IN PHYSICS.

June 1997
ADDIS ABABA

## ACKNOWLEDGEMENT

I would like to express my gratitude to my advisor Dr. Th. Eickhoff for his consistent advice and friendly encouragement throughout my work in KFA Juelich Germany.

I am greatly indebted to my home advisor prof. R.Y. Thakur for his advice, valuable comments and suggestions.

I would like to thank Ms. K. Winz for her practical assistance and unreserved help throughout my work.

I also thank my friend Kifle Gebre for printing the first & final version of the thesis and W/t Emebet Legesse for typing the thesis on the computer.

Finally, I would like to thank DAAD for financing my living expense during my six month stay in Germany.


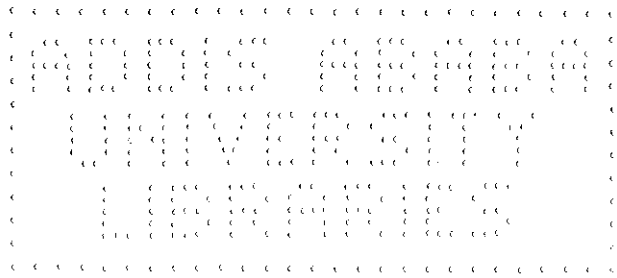

# CONTENTS

## ABSTRACT

Reflectance(R), Transmittance(T), and Scattering distribution of thin film TCOs and with their p-/ (thin & thick) i-layer stacks have been measured for various wavelengths. The shape of scattering distributions have been determined by using an easy plot software. The functional dependence of normalised intensity on wavelength ($\lambda$) and scattering angle ($\theta$) have been determined for Asahi U & Standard TCO. The thickness of individual layers was determined from reflectance & transmittance measurements by using an optical simulation software for layer stacks. The diffused transmittance determined from transmittance measurement and scattering distribution measurements have been compared.

# 1. General Introduction

Energy and environment are presently two important issues in the world. Renewable energy is the answer to the energy problem without polluting the environment. Solar energy is the most renewable and abundant energy source. Every year the sun gives to the earth $1.5 \times 10^{18}$ kwh/yr [1].

A solar cell is a device which converts sunlight directly into electricity. Hydrogenated amorphous silicon solar cells make use of the photovoltaic effect. The first a-Si:H solar cell was reported by Carlson and Wronski with an initial conversion efficiency of 2.4% in 1976. Since that time much research has been carried out, various technologies have been developed for a-Si:H solar cells. The initial conversion efficiency of a-Si:H solar cells has been raised to more than 13% for a single junction cell [1] and a new world record stable conversion efficiency of 11.8% [2] for amorphous silicon alloy solar cells have been achieved in triple junction structure by United Solar System Corp.(USSC) in 1996.

Today a-Si:H based solar cell technology has become a leading candidate for large area, low-cost photovoltaic application. The area of a-Si:H solar cell is not limited by the a-Si:H material but by the substrate size. It is possible to fabricate a-Si:H solar cells on different kinds of substrates, such as: glass, polymer, stainless steel foil, etc.[1]. A-Si:H solar cells can be adapted for various applications. They can be integrated into tiles (with different forms and colours). They can be made transparent to be integrated in windows and car sun roofs. A-Si:H solar cell have already found their way into powering pocket calculators, battery chargers, watches, car ventilation fans, etc.

Currently the main issues in the a-Si:H solar cell fields are to further improve the low conversion efficiency & the stability of solar cells against the light induced degradation, and to find a cost effective way of mass production.

The main cause for low conversion efficiency in an a-Si:H solar cell is light losses. To minimise the light loss, light trapping mechanism should be developed. The proposed light trapping mechanisms are discussed in section (1.5). The study of light trapping effect in a-Si:H solar cells is important for two major reasons. Firstly, the electrical properties of a-Si:H based materials can no longer be much improved with the present technology in order to achieve a

better solar cell performance. Secondly, it may lead us to some break through in the solar cell research by enabling us to optimise the cell structure optically. However, theoretical study of the optical aspects in a-Si:H solar cells is very complex.

In this work section one introduces the properties of layers, light losses, and light trapping mechanism in an a-Si:H solar cell. In section two the theory of reflectance, transmittance, absorption, Fresnel relations, in particular the experimental determination of the diffused reflectance and transmittance are discussed. Section three contains the list of experimental apparatus and the procedures to carry out the measurements. In section four the experimental results and their interpretations are given. And finally in section five and six conclusion and list of reference materials are stated respectively.

## 1.1 What is roughness?

It is important to discuss what is meant by surface roughness even though we did not measure the roughness of our sample. Roughness is a measure of the topographic relief of a surface [3]. Surface relief includes polishing marks on optical surfaces, machining mark on machined surfaces, etc.

Fig. (1.1) shows the schematic representation of a rough surface and some parameters used for describing the surface. Surface height variations are measured from mean surface level and expressed as an rms roughness value (δ). The separation between similar surface features along the surface is referred to as surface spatial wavelength or statistically as correlation length [3].

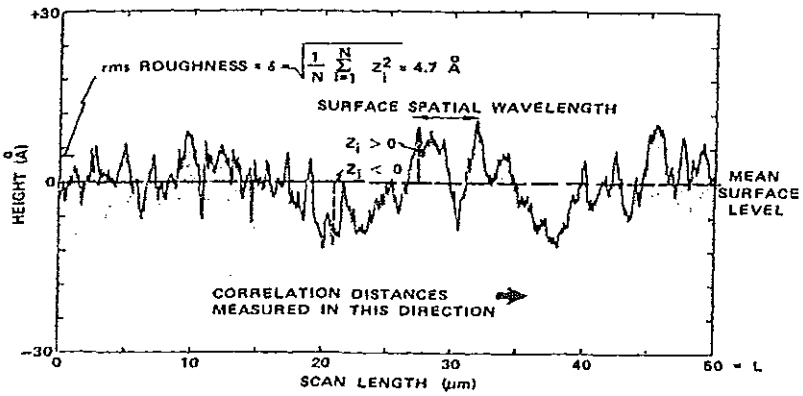


Fig 1.1. Schematic representation of a rough surface.

There is no unique rms roughness for a surface. It depends on the length of surface profile (maximum spatial wavelength), the surface area being averaged over for each measurement and the distance between data points.

One can see roughness by observing light scattered by the surface, by using a differential interference contrast (Nomarski) microscope or by using electron microscopes.

Dust particles and particulates are not part of the intrinsic surface roughness, if they appeared on the surface of the sample they influence the scattering distribution. One has to clean the samples before performing a scattering measurement.

## 1.2 The structure of an a-Si:H Solar Cell

The structure of a conventional a-Si:H Solar cell is shown in fig(1.2.). First a transparent conductive oxide (TCO) layer is deposited on a glass substrate. The glass substrate has a thickness of around (1-2)mm and is used to support thin films of the solar cell. The TCO layer will act as front contact of the cell. After the TCO layer is deposited, different types of hydrogenated amorphous silicon layers are deposited one after another. These layers are the boron doped p-layer, the undoped intrinsic i-layer and the phosphorous doped n-layer. Finally a metal layer is deposited as the back contact. The solar cell now has a glass /TCO/ PIN/ metal structure and is complete.

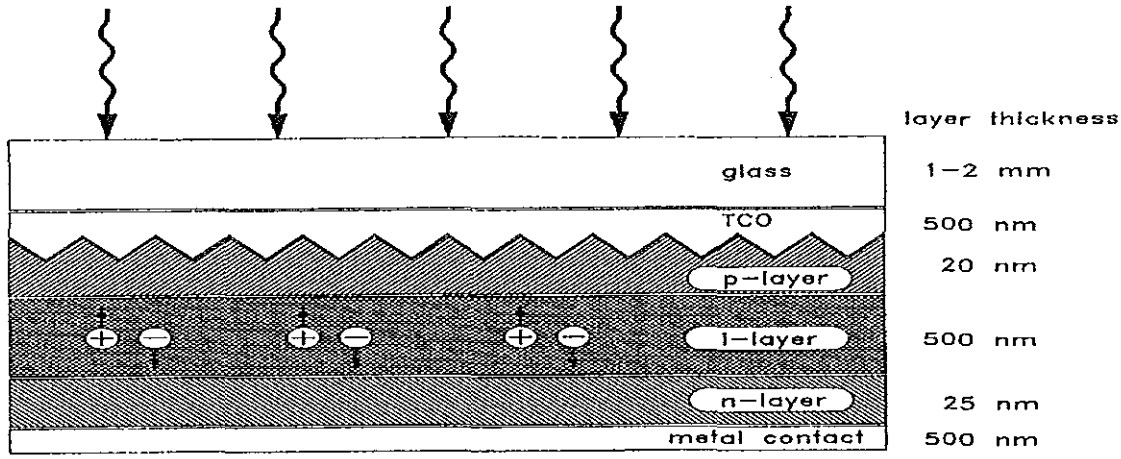


Fig. 1.2 The structure of a conventional a-Si:H solar cell.

In photovoltaic process the photons which are absorbed in the pin layers generate electron-hole pairs. These electron-hole pairs are separated by the internal field provided by p- and n-layers and collected at the electrodes. Thus a current and/or voltage can be obtained in external circuits.

## 1.3 Thin layers in an a-Si:H Solar Cell

### 1.3.1 The TCO

The TCO (transparent conductive oxide) layer acts as a front ohmic contact for the solar cell. As a front contact, it should satisfy the following:

i) It should be highly conductive. Any resistance in the TCO layer will contribute to the series resistance of the solar cell, which deteriorates the solar cell performance.

ii) It should be highly transparent and have suitable refractive index. Any light absorbed in the TCO layer will not contribute to the electrical output.

iii) It should be able to make ohmic contact to the P-layer. The resistance of ohmic contact should also be as small as possible.

Several materials are used as TCO for example indium tin oxide (ITO) (tin doped indium oxide $InO_2$:Sn), Fluorine doped tin Oxide ($SnO_2$:F), Aluminum or boron doped Zinc oxide (ZnO:Al, ZnO:B), water sputtered Zinc oxide. ITO, $SnO_2$ and ZnO have similar refractive indices and small extinction coefficients [1]. They are suitable materials for the front contact. TCOs we have used for our work are Fluorine doped Tin oxide and water sputtered zinc oxide. All the TCOs we have used have different texture and thickness.

### 1.3.2 The P-layer

The P-layer used in a-Si:H solar cell is boron doped amorphous silicon. It should have a wide optical gap as compared to the intrinsic layer (i-layer) so that most of the light will reach i-layer without being absorbed by the P-layer. The light absorbed in the P-layer only slightly contributes to the electrical properties of solar cell due to the existence of large number of recombination centers. For this reason the P-layer is considered as an optically dead layer for solar cells.

Since boron doping decreases the optical gap of a-Si:H [4], carbon alloying is used to increase the optical gap of the P-layer. The optical gap of P-layer used for a-Si:H solar cell is around 1.92 eV. The thickness of the P-layer should be small in order not to absorb light passing through it. The thickness of the P-layer we used for our measurement is 15nm, it was determined by using a Window version simulation software for variable angle spectroscopic ellipsometer (W.V.A.S.E.) from near normal incidence spectra.

### 1.3.3 The i-layer

The i-layer is the optically active layer for solar cells for a typical a-Si:H. It has a thickness of 500nm and an optical gap of 1.7eV. It is optically active because light absorbed in this region creates electron-hole pair in order to have short circuit current and open circuit voltage.

Light trapping in the i-layer could be improved by increasing its thickness, decreasing its optical band gap and increasing reflectance of back metallization [4]. Even though increasing thickness of the i-layer increases the light absorption, it will result in a decrease in quantum efficiency of the solar cell. The reason is that as the thickness increases the probability of generated electron-hole pair to recombine will increase and thus short circuit current will decrease.

### 1.3.4 The n-layer

The n-layer used in a-Si:H solar cell is phosphorous doped microcrystalline hydrogenated silicon ( μc-Si:H). The optical gap of the n-layer is the same or slightly smaller than that of the i-layer. The light entering the n-layer (long wavelength light) need not be absorbed by the n-layer because the light absorbed by the n-layer will not contribute to the electrical output of the solar cell. The reason is that the absorbed light generates electron-hole pair but the generated electron-hole pairs recombine due to the existence of a large number of recombination centers. For this reason it is considered as an optically dead layer for the solar cell.

### 1.3.5 The metal layer

The metal layer is employed as a back contact of the solar cell. As a back contact it should be [1]

i) highly reflective (to the a-Si:H layers) especially for long wavelength light ($550nm \leq \lambda \leq 800nm$). The reflectivity is less important for the short wavelength light, because it is already absorbed in the i-layer before reaching the back contact. However, some light with long wavelengths still reaches the back contact. Any light further transmitted into the metal layer and absorbed there does not contribute to the electrical output.

ii) able to make ohmic contact with the n-layer. The resistance of the ohmic contact should also be as small as possible. Since metals are good conductors the series resistance of the metal layer can be neglected. Aluminum (Al) and silver (Ag) are frequently used as a back contact. Aluminum is cheap while silver is expensive but the reflectivity of silver is higher than that of aluminum. Silver can be easily oxidized in the atmosphere which makes it a less stable material. A double layer Ag/Al could be used so that silver gives high reflectivity and the Aluminum layer protects the silver layer.

## 1.4 Light loss in an a-Si:H Solar Cell

The conversion efficiency of a - Si:H solar cell is not satisfactory. The main cause for the low conversion efficiency is due to optical losses.

### 1.4.1 Reflection at the front

The reflectance at the front for smooth layers can be easily calculated by thin film optics. In the normal incidence case which gives least reflectance at an interface, the reflectance only depends on the refractive indices of the media of the two sides of the interface [1].

$$R = \left| \frac{n_1 - n_2}{n_1 + n_2} \right|^2$$

The refractive indices of glass, TCO and P-type a-Si:H layers are 1.5, ~ 2, and ~3.5 respectively. The reflectances are 4%, 2% and 8.2% for the air/glass, glass/TCO and TCO/p-a-Si:H interfaces respectively. Reflectance at the front of the solar cell depends on the wavelength.

### 1.4.2 Transmission at the back contact

The transmission loss at the back contact is strongly wavelength dependent. Because a-Si:H layers are thin, a large fraction of light with long wavelength ($\geq$ 650 nm) is still not absorbed after passing through a-Si:H layers and reaches the back contact. Since the back contact is not an ideal optical reflector, part of the light will penetrate the metal layer which does not contribute to the photovoltaic process.

Absorption in other layer such as TCO, p-layer and n-layer can also cause optical losses. The absorption in the P- and n-layer are material dependent.

## 1.5 Methods of light trapping in an a-si:H solar cell

Light trapping in an a-Si:H solar cell means to trap light in the intrinsic layer so that the light is absorbed there and converted to electricity. Light trapping involves:

i) minimising reflection loss at the front and transmission loss at the back interfaces

ii) enlarging the optical path without increasing the geometrical thickness.

iii) minimizing the absorption in the TCO, P-layer and n-layer.

Methods of light trapping can be described under the following categories.

### 1.5.1 Textured cell structure

The most common method to achieve light trapping in an a-Si:H solar cell is to use a textured cell structure. The textured TCO substrate is employed and p-i-n layers are deposited in sequence. The key words for the light trapping in textured cells are light scattering at rough interfaces which will be discussed in detail in section 2.2.

### 1.5.2 Highly reflective back contacts

In order to overcome the transmission and absorption loss at the back of the solar cell a highly refractive material/reflective metal double layer back contact can be applied. The purpose of a highly refractive rear window layer is to bend the reflected light by the metal on the way it enters the hydrogenated silicon layer. The more light is refracted into the hydrogenated silicon layer, the longer is the path length inside this layer and thus the higher is the probability of light being absorbed . Zinc Selenide (ZnSe) and Zinc Sulfide (ZnS) as well as alloys of the two are two very promising candidates for rear window layers. [6,5]

### 1.5.3 Tandem Cell Structure

The employment of a tandem cell structure is mainly for the stability of solar cells. To overcome Staebler-Wronski effect, the i-layer in the p-i-n structure should be thin. However, we need an i-layer with some degree of thickness to absorb enough light. The tandem cell structure consists of two p-i-n structures on top of each other. In a tandem cell structure, i-layers of different materials can be used to absorb enough light, thus benefitting from

a wider spectral range of the sun light. Hydrogenated amorphous silicon germanium (a-SiGe:H) is one of the suitable candidates.

### 1.5.4 V-Grooved Structure

In the V-grooved structure the glass substrate is first grooved to make a V-form [1,6,7]; and then the TCO and a-Si:H layers are deposited. The dimensions of the V-groove is much larger than the a-Si:H layer thickness. A schematic drawing of this structure is shown in fig(1.3). The light trapping process in such cells is as follows: when light enters through the glass and reaches the glass/TCO/a-Si:H interface will reach the opposite side and re-enter the cell there. In this V-groove structure, every facet is relatively smooth. Thus, such cells are expected to have a good electrical performance because of smooth facets. It is also believed that these cells may suffer less from light induced degradation because a thinner intrinsic layer can be used.

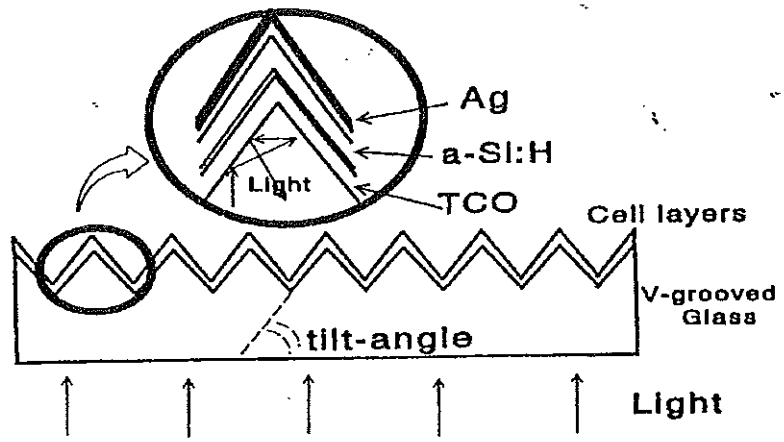


Fig(1.3) The structure of a V-grooved cell.

# 2 Thin Film Optics

Thin Film optics is very important in studying the optical properties of a-Si:H based solar cells. This chapter deals with reflection, transmission and absorption of light.

## 2.1 Reflection and Transmission at a flat interface

When light reaches a smooth (flat) interface in the normal direction, part of the light is reflected back and part of it is transmitted. The reflectance and transmittance can be determined with the help of the Fresnel amplitude coefficients.

$$\tilde{r} = \frac{\tilde{n}_0 - \tilde{n}_1}{\tilde{n}_0 + \tilde{n}_1} \qquad 2.1.1$$

$$\tilde{t} = \frac{2\tilde{n}_0}{\tilde{n}_0 + \tilde{n}_1} \qquad 2.1.2$$

Where $\tilde{n}_0$ is the refractive index of the first medium,

$\tilde{n}_1$ is the refractive index of the second medium,

$\tilde{r}$ and $\tilde{t}$ are the Fresnel amplitude coefficients in reflection and transmission respectively.

If the media are absorbing the refractive index will be complex. It will have real and imaginary part.

$$\tilde{n}_0 = n_0 + i\kappa_0 \qquad 2.1.3$$

$$\tilde{n}_1 = n_1 + i\kappa_1 \qquad 2.1.4$$

Equations (2.1.3) and (2.1.4) are complex indices of refraction of the first and second medium. $\kappa_0$ and $\kappa_1$ are extinction coefficients of the first and second medium.

The reflectance and transmittance are:

$$R = \tilde{r}\tilde{r}^* = \left(\frac{\tilde{n}_0 - \tilde{n}_1}{\tilde{n}_0 + \tilde{n}_1}\right)\left(\frac{\tilde{n}_0 - \tilde{n}_1}{\tilde{n}_0 + \tilde{n}_1}\right)^* \qquad 2.1.5$$

$$T = \frac{\tilde{n}_1}{\tilde{n}_0}\tilde{t}\tilde{t}^* = \frac{\tilde{n}_1}{\tilde{n}_0}\left(\frac{2\tilde{n}_0}{\tilde{n}_0 + \tilde{n}_1}\right)\left(\frac{2\tilde{n}_0}{\tilde{n}_0 + \tilde{n}_1}\right)^* \qquad 2.1.6$$

If the medium through which light is incident on the interface is air and refracted from the interface to an absorbing medium of refractive index $\tilde{n}_1$. Therefore $n_o$ is assumed to be real. For an absorbing substrate $\tilde{n}_1$ should be replaced by its complex representation $\tilde{n}_1 = n + i\kappa$. Thus equations (2.1.5) and (2.1.6) can be written as

$$R = \frac{(n - n_0)^2 + \kappa^2}{(n + n_0)^2 + \kappa^2} \qquad 2.1.7$$

$$T = \frac{4n_0(n - i\kappa)}{(n + n_0)^2 + \kappa^2} \qquad 2.1.8$$

From conservation of energy the sum of reflectance and transmittance should be unity for non-absorbing mediums i.e.

$$R + T = 1 \qquad 2.1.9$$

While if one of the media is absorbing then equation (2.1.9) will include the absorption ($A$) of the absorbing medium. We shall then have

$$R+T+A=1 \qquad 2.1.10$$

## 2.2 Reflection and Transmission at a slightly rough interface

When light reaches a rough interface, part of the light will be reflected and transmitted in specular direction, the other part will be diffusely reflected and transmitted. All the light returned by the surface may be viewed as reflected light: the specularly reflected light as coherently reflected and scattered light as incoherently reflected [1].

We denote the specular reflectance as $R_s$, specular transmittance as $T_s$, the diffused reflectance as $R_d$, and the diffused transmittance as $T_d$. For non-absorbing medium, energy conservation leads to

$$R_s + R_d + T_s + T_d = 1 \qquad 2.2.1$$

If one of the medium is absorbing, then equation (2.2.1) should include the absorption ($A$) of the absorbing medium, we shall then have

$$R_s + R_d + T_s + T_d + A = 1 \qquad 2.2.2$$

In general, the amount and angle distribution of scattered light do not only depend on the refractive indices of the media; but also on the interface roughness and the incident angle. For rough interfaces with known morphology, one can apply geometrical optics or electromagnetic theory to calculate the light scattering. Because the morphology of rough interfaces is usually random, it is very difficult to solve the Maxwell's electromagnetic equation for such a system.

Scalar scattering theory can be used to calculate a value of effective rms surface roughness [1]. Three types of measured reflectance are used in the calculation: specular reflectance $R_s$, diffuse reflectance $R_d$ and total reflectance $R_o$. The relation between them is

$$R_o = R_s + R_d.$$

The scalar scattering theory relates the specular reflectance $R_s$ of a surface and total reflectance $R_o$ to the rms roughness ($\delta$), incident wave length $\lambda$, and incident angle $\theta_0$.

$$\frac{R_s}{R_0} = \exp-\left(\frac{4\pi\delta n_0 \cos\theta_0}{\lambda}\right)^2 \qquad 2.2.3$$

For a rough surface where the diffusely reflected light $R_d$ is more than 1% of the total reflected light, the ratio of specular to the total reflectance of a surface is preferably calculated directly from equation (2.2.3) [1]. It is also possible to take the ratio of diffuse reflectance to the total reflectance.

$$\frac{R_d}{R_0} = \frac{R_0 - R_s}{R_0} = 1 - \exp-\left(\frac{4\pi\delta n_0 \cos\theta_0}{\lambda}\right)^2 \qquad 2.2.4$$

At normal incidence and $\delta << \lambda$ equation (2.2.4) can be reduced to

$$\frac{R_d}{R_0} = \left(\frac{4\pi\delta n_0}{\lambda}\right)^2 \qquad 2.2.5$$

However, there is no similar formula found in literature for transmittance. Smith [8] and Tao[4] assumed that the diffused transmittance $T_d$ was related to diffused reflectance $R_d$ through a scattering parameter $C$.

$$T_d = CR_d \qquad 2.2.6$$

For $\delta \approx \lambda$, $C>1$; for $\delta << \lambda$, $C \approx 1$, $C$ should be constrained by $C \le \frac{1}{R_s + R_d} - 1$ which is required by the non-negative value of $T_s$. With these constraints, for $\delta < \lambda$, $C$ can be expressed as

$$C = \exp\left(\frac{C_0\delta}{\lambda}\right) \qquad 2.2.7$$

$C_0$ is a positive number of the order of one.

As a special case, when δ=0, from equation (2.2.4) we have $R_s = R_o$ which is the same as the case of flat interfaces. We assume $R_s + R_d$ equals the $R_o$ of a flat interface (between the same media). This also means $T_s + T_d$ equals $T_0$ of the corresponding flat interface.

The above discussion holds true for a single interface. But in solar cells there are a number of interfaces. For multiple interfaces theoretical analysis of reflectance and transmittance are explained in [4,18,19] which is beyond the scope of this paper. But experimentally we can determine the total reflectance and transmittance and the diffused reflectance and transmittance for multiple rough interfaces.

## 2.3 Experimental determination of total & diffused reflectance and transmittance

According to experimental procedure in section (3.4) one can measure the intensity of incident light $I_0$ before putting the sample and by putting the sample on the sample holder in such a way that light falls on the glass side of the sample. Then one can measure the transmitted intensity $I_t(\theta)$. Here $\theta = 0$ corresponds to directly transmitted light and the intensity at $\theta > 0$ corresponds to scattered (diffusely transmitted intensity). This measurement also collects multiply reflected and transmitted intensities. Thus the ratio of the transmitted intensity to the intensity of incident light is transmittance. The specular transmittance can be defined as

$$T_s = \frac{I_t(0)}{I_0} \qquad 2.3.1$$

and the diffused transmittance at any scattering angle θ for $\theta > 0$ is

$$T_d(\theta) = \frac{I_t(\theta)}{I_0} \qquad 2.3.2$$

Thus the total transmittance $T_o = T_s + T_d$ and the total transmittance $T_o$ can be determined by the equation.

$$T_0 = \int_0^{2\pi} \int_0^{\pi/2} T(\theta)\sin(\theta)d\theta d\varphi \qquad 2.3.3$$

where $T(\theta)$ is the normalised intensity which has to be measured just when light emerges from the sample but that is difficult to achive. We have measured the intensity at a distance $R$ from the sample. Thus the normalised intensity measured at a distance $R$ is reduced by the factor of solid angle $\Delta\Omega$ as shown in fig.(2.1)

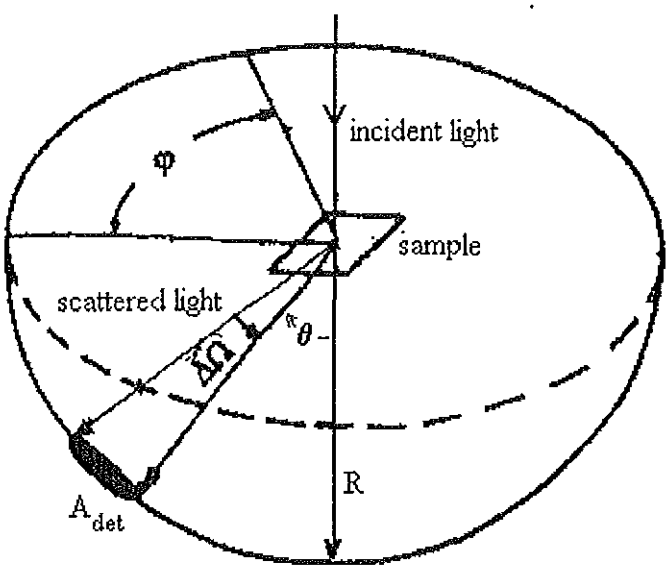


Fig. 2.1 Schematic representation of the scattered intensity measurement over the half sphere.

$$T_{measured}(\theta)=T(\theta)\Delta\Omega \qquad 2.3.4$$

Thus the geometrical factor $\Delta\Omega$ related to the effective area of the detector $A_{det}$ and the distance from the sample to the detector $R$ is given by

$$\Delta\Omega = \frac{A_{det}}{R^2} \qquad 2.3.5$$

Thus equation (2.3.3) can be written as

$$T_0 = \frac{R^2}{A_{\text{det}}} \int_0^{2\pi} \int_0^{\pi/2} T_{measured}(\theta) \sin\theta d\theta d\varphi \qquad 2.3.6$$

If the normalised scattered intensity is isotropically distributed over the half sphere (independent of the angle φ)

$$T_0 = \frac{2\pi R^2}{A_{\text{det}}} \int_0^{\pi/2} T_{measured}(\theta) \sin\theta d\theta \qquad 2.3.7$$

Experimentally the diffused transmittance can be determined in the following way. First one can fit the measured normalised intensity versus scattering angle curve for $\theta \geq 10^0$ to be sure that no specularly transmitted light is detected and then the model fit curve can be extrapolated to $\theta = 0^0$. Let us denote the extrapolated fit curve by f(θ). Thus taking geometrical factor in to consideration the diffused transmittance is given by

$$T_d = \frac{R^2}{A_{\text{det}}} \int_0^{2\pi} \int_0^{\pi/2} f(\theta) \sin\theta d\theta d\varphi \qquad 2.3.8$$

If the normalised scattered intensity is isotropically distributed over the half sphere (independent of scattering angle φ)

$$T_d = \frac{2\pi R^2}{A_{\text{det}}} \int_0^{\pi/2} f(\theta) \sin(\theta) d\theta \qquad 2.3.9$$

The difference between the total transmittance measured by an integrating sphere and specular transmittance measured by spectrophotometer is the diffused transmittance. This diffused transmittance can be compared with the result obtained using equation (2.3.9). The comparison is given in section four. Similarly one can determine the total and diffused reflectance experimentally.

Fig.2.2 shows how to find the diffused transmittance from the measured (experimental) normalised intensity versus scattering angle θ curve for Asahi U sample at λ = 400nm. In this graph the extrapolated model fit curve is denoted by $f(\theta)$ and θ is given in radians. Thus the integral $\int_0^{\pi/2} f(\theta)\sin(\theta)d\theta$ is the area bounded by the $f(\theta)\sin(\theta)$ curve with the θ-axis.

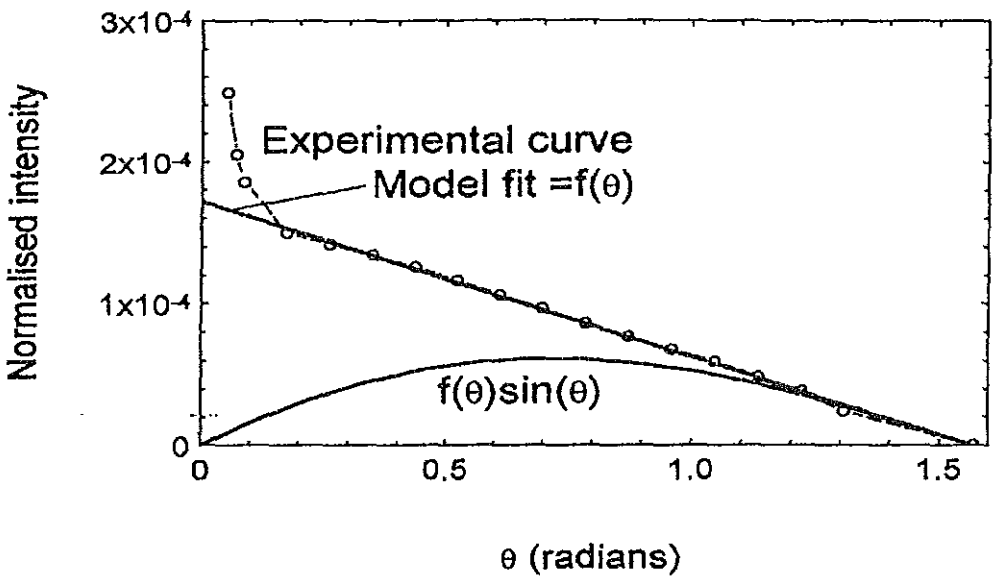


Fig 2.2 The measured normalised intensity for Asahi U at λ = 400nm together with the model fit curve $f(\theta)$ and $\sin(\theta)$.

To get equation (2.3.9) from equation (2.3.8) one has to check whether the scattered intensity is isotropically distributed or not. We have checked that in the following way; we measured the scattering of our sample, and then without changing anything else we rotated our sample by angle φ about the z-axis in such a way that the illumination area was not changed. We then measured the scattering distribution, and no difference was observed. This told us that the scattering distribution was φ independent, so that we used equation (2.3.9) to determine the diffused transmittance.

The geometrical factor was found to be $\Delta\Omega = 1.056\text{x}10^{-3}$ with 4.7% error and it was used throughout our work to determine the diffused transmittance. The integral in equation (2.3.9) was evaluated by using an easyplot windows software. The diffused transmittance calculated by using equation (2.3.9) was 0.274, while the measured value by using spectrophotometer was 0.241. Thus the relative deviation of calculated value from the measured value was 12 %. The cause for these deviation could be the effect of neutral density filters and error in determining the geometrical factor.

The main purpose of using rough TCO layers and rough layer stacks is to have light scattering which enables the light to travel a longer path in the solar cell. The longer the path the light travels in the solar cell, the higher the probability of being absorbed. Therefore let us discuss about optical absorption in a-Si:H solar cell.

## 2.4 Optical absorption

Radiation absorption occurs in the bulk of the media. If multiple scattering is negligible the irradiance of a beam of light is exponentially attenuated from $I_i$ to $I_t$ in traversing a distance $h$ through a particulate medium [11].

$$\frac{I_t}{I_i} = \exp(-\alpha h) \qquad 2.4.1$$

where $I_i$ is the irradiance at an interface ($h$=0) and $\alpha$=2$\omega\kappa$/c is the absorption coefficient.

Absorption is a phenomenon of fundamental interest because of its relation to the dynamics of electrons and ions of the medium under the influence of electromagnetic radiation [12]. An absorbing medium is characterised by a complex dielectric constant $\varepsilon = \varepsilon_1 + i\varepsilon_2$ and a complex refractive index $n + i\kappa$. It follows from Maxwell's equation (for the free electron case) that

$$(n+i\kappa)^2=\varepsilon_1+i\varepsilon_2 \qquad 2.4.2$$

Absorption takes place because of the interaction between photons and the conduction (free) electrons as in the case of metals or because of bound electrons associated with the interaction between photons and the natural frequency of vibration(phonons).

Absorption in an a-Si:H film could be described in the following [13].

1. For $\alpha > 10^3$ $cm^{-1}$, absorption is believed to take place between extended states and is often described by Tauc's expression.

$$(\alpha\hbar\omega)^{1/2} = B(\hbar\omega - Eg) \qquad 2.4.3$$

This relation is commonly used to define the optical gap $Eg$(opt) of the material.

2. For $\alpha<10^3 cm^{-1}$, there is an exponential dependence of $\alpha$ on the energy (Urbach tail):

$$\alpha=\alpha_0 \exp[-(E-E^*)/E_0] \qquad 2.4.4$$

where Eo is the width of the urbach tail and $E^*$ is the energy intercept.

3. In the low energy range, the curves flatten off and $\alpha$ depends sensitively on the details of preparation process, doping level, and defect density. This shoulder, is therefore ascribed to defect absorption [13,14].

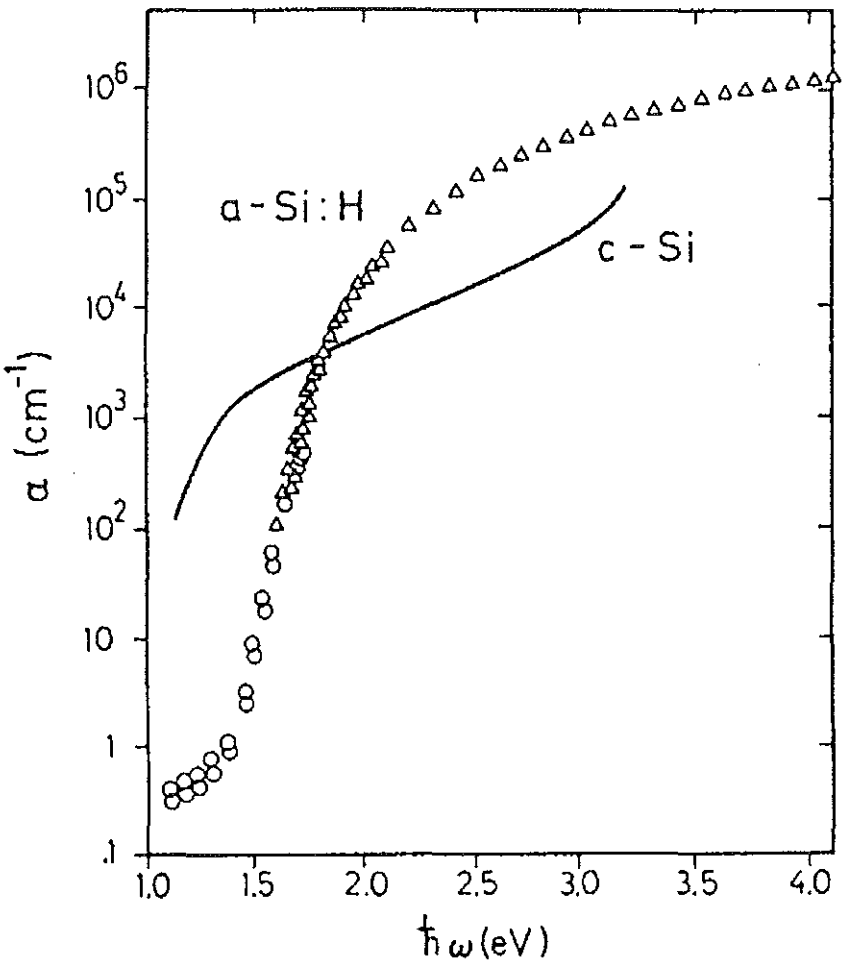


Fig(2.2) Absorption coefficient of a-Si:H derived from optical absorption (Δ) and photoconductivity (o)[13].

# 3. Experimental Details

## 3.1 Sample preparation

We have used four kinds of TCOs for our work. These are:

i) Flat TCO of film thickness 90nm. It has a smooth surface.

ii) Standard TCO of film thickness 500 nm. It has a rough surface.

iii) Asahi U TCO of film thickness 800nm. It has a rough surface. Asahi is one of the Japanese glass companies and U is the type of TCO prepared by this glass company.

iv) Water sputtered Zinc Oxide. We have used three kinds of Zinc Oxide which had been prepared with different water partial pressure and at the same heater temperature of $330^0$C. They are identified by their identification number (22-47, 22-51, & 20-38 ).

a) 22-47 has a thickness of 1190 nm and had been prepared with the water partial pressure of $6.1 \times 10^{-6}$ torr. It is less hazy.

b) 22-51 has a thickness of 1095nm and had been prepared with the water partial pressure of $1.2 \times 10^{-4}$ torr. It is rough as compared to 22-47.

c) 20-38 has a thickness of 1260 nm and had been prepared with the water partial pressure of $1.1 \times 10^{-3}$ torr. It is rough as compared to 22-47 and 22-51.

One piece from all the TCOs were taken for reflectance, transmittance and scattering distribution measurements.

One piece from all the TCOs were taken and treated with hydrogen for half minute in a 6-chamber plasma enhanced Chemical Vapor Deposition (PECVD) machine.

We treated our samples with hydrogen to see the effect of hydrogen on the optical properties of TCOs.

One piece each from the first three TCOs were taken and deposited with 15 nm p-layer on top of the TCOs.

One piece each from the first three TCOs were taken and deposited with 15 nm p-layer on top of the TCOs and 50 nm i-layer on top of the p-layer.

Finally one piece each from the first three TCOs were taken and deposited with 15nm p-layer on top of the TCOs and an additional 380 nm i-layer on top of the p-layer.

The hydrogen treatment and layer deposition were performed by deposition group in KFA at the institute of thin film and ion technology ISI-PV Juelich. The Zinc oxide TCO substrates were prepared by Oliver Kluth in KFA Germany. He is one of the PH.D. students in KFA.

## 3.2 Near normal Incidence Specular Reflectance and Transmittance measurement

We have used a Perkin Elmer Lambda 19 UV/VIS/NIR double beam spectrophotometer. It is a fast and powerful machine for reflectance and transmittance measurement. It has two detectors: one to detect in the UV and Visible region and the other to detect in the NIR region. It measures the ratio of the intensity of the sample beam to the reference beam.

### a) Reflectance measurement

i) Spectrophotometer was switched on and we waited for about 20 minutes so that the lamps reach their thermal equilibrium.

ii) Reference and sample beam reflectance holders were mounted. By putting standard mirrors on both reflectance holders the instrument background correction was performed.

iii) The mirror on the sample beam was replaced by the sample and measurement was performed.

iv) Finally the measured reflectance in step(iii) was multiplied by the reflectance of the standard mirror.

### b) Transmittance Measurement

i) After putting a transmittance holder on the sample beam, the instrument background correction was performed.

ii) The sample was put on the sample holder in such a way that light impinges from the glass side; and measurement was performed. The transmittance curve was displayed on the screen.

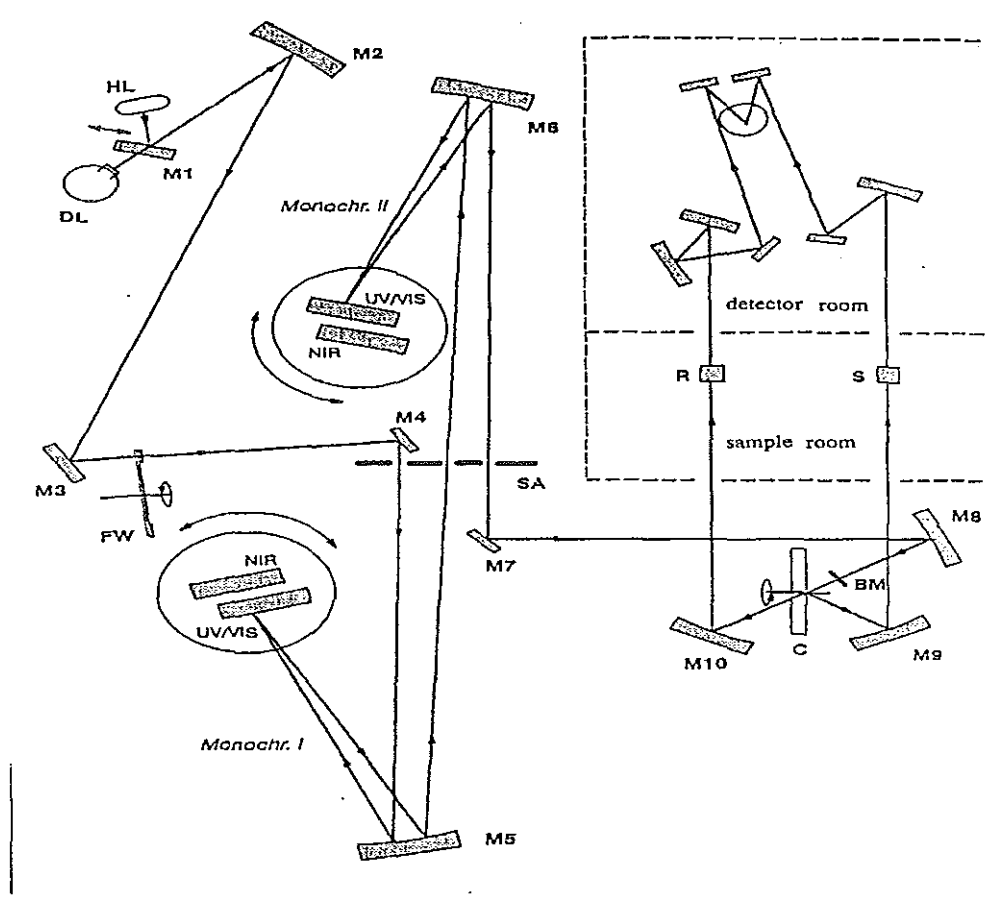


Fig 3.1 Optics of spectrophotometer.

| | |
|---|---|
| FW is filter wheel | HL is halogen lamp |
| DL is deutirium lamp | M(1-10) are reflecting mirrors |
| R is reference beam | S is sample beam |
| C is chopper | BM is beam mask |

## 3.3 Total Reflectance and Transmittance measurement by using Integrating sphere

This is the same experimental set up as with the spectrophotometer except that the normal compartment was replaced by the integrating sphere. The inner part of the integrating sphere is made up of white material so that it diffuses light falling on its surface nearly to 100%. The integrating sphere has sample mounting ports for reflectance and transmittance measurements. It is designed to collect all the scattered and non-scattered light both in reflectance and transmittance measurements. The measurement was performed according to the following procedure:

i) Spectrophotometer was switched on and we waited for about 20 minutes so that the lamps reach their thermal equilibrium.

ii) Standard reference material was put at the reflectance sample holder and instrument background correction was performed.

iii) Transmittance was measured by putting the sample at the transmittance holder and the transmittance curve was displayed on the screen.

iv) For reflectance measurement the reference material at the reflectance holder was replaced by the sample to be measured and measurement was performed. Behind the sample there was black material that can absorb the transmitted light nearly to 100%. Reflectance curve was displayed on the screen.

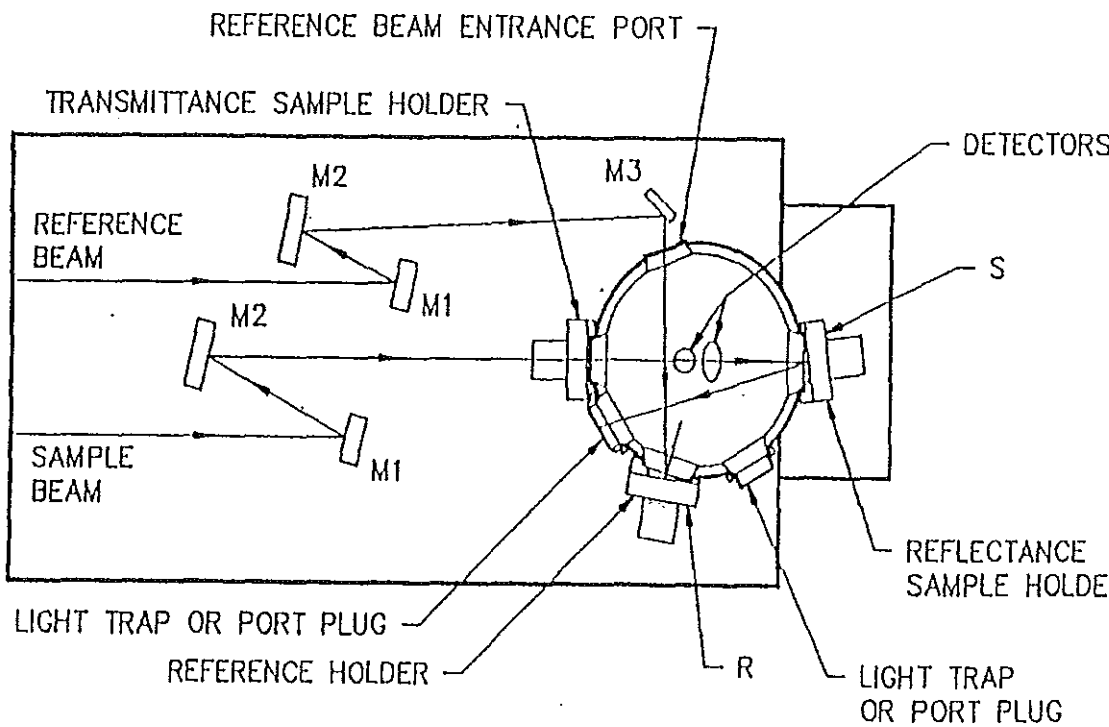


Fig.3.2 Optics of integrating sphere.

## 3.4 Angle-Resolved transmittance measurement by using GonioPhotometer

Goniophotometer is a device used to measure the transmitted and reflected light intensity at different scattering angles. It can measure directly transmitted and reflected light intensity and diffusely transmitted and reflected light intensity in units of mV. It has a light source, and optical glass fibers to transport light from the source to the sample and

from the point of collection of transmitted light to the monochromator. The transmitted light was detected by the detector after it had passed the monochromator.

i) The power source was switched on and we waited for about 20 minutes until the Xe lamp reaches its thermal equilibrium.

ii) The position of the sample holder was adjusted in such a way that the distance from the sample to the detector at any angle θ was the same.

iii) At normal the incidence the intensity of incident light was measured by putting neutral density filters of optical density D on the sample holder.

Neutral density filter can attenuate the incident light intensity. It will attenuates the intensity of incident light if its optical density is greater than one. Optical density D is defined as the logarithm to the base 10 of inverse of transmittance of neutral density filters[15,16].

$$D = \log_{10}\left(\frac{1}{T}\right) \quad or \quad T = 10^{-D}$$

To get the intensity of the incident light, one has to divide the measured value by the transmittance of neutral density filters given by $T = 10^{-D}$, but the actual value of T depends on the wavelength. For our work, we had measured transmittance of neutral density filters for the desired wavelength by using spectrophotometer.

iv) The samples were cleaned from any dust particles before performing scattering distribution measurement.

v) The sample was placed on the sample holder in such a way that light was incident on it at right angle to its surface.

vi) The intensity of transmitted light was measured for every (five)5 degree interval. Zero corresponds to directly transmitted light. The experiment was performed for visible light.

vii) Ellipsometeric software was used to move the detector and the source to the desired angle and monochromater to the desired wavelength.

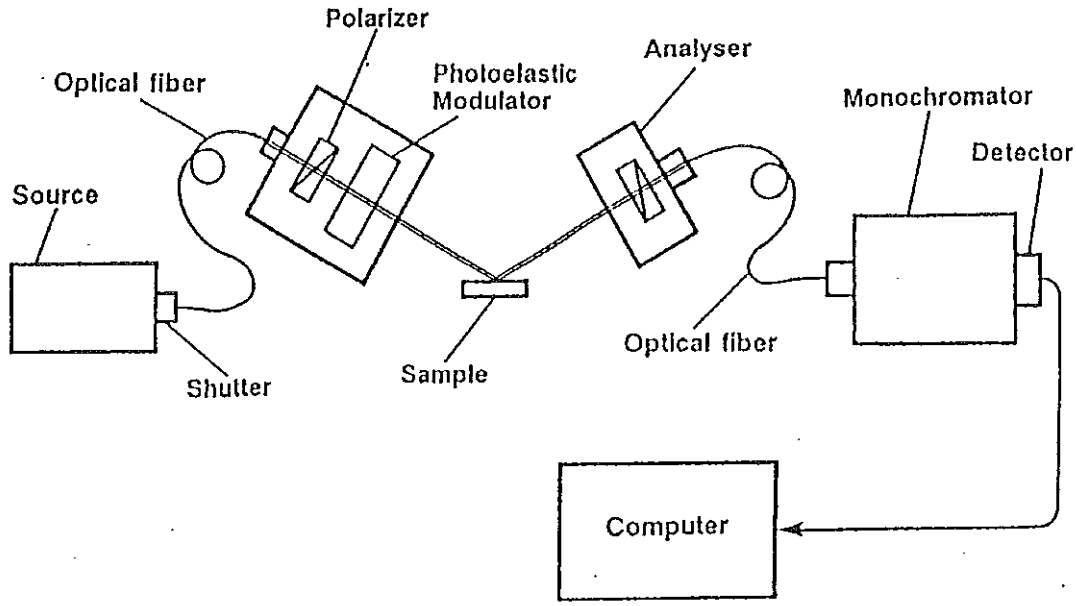


Fig.3.3.GonioPhotometer

# 4. RESULTS AND DISCUSSION

In some of the spectra displayed in this section the dot points on the diffused transmittance curves are those found by using equation (2.3.9) and the dot points on the specular transmittance curves are those found by using equation(2.3.1).

We have omitted in our work the n a-Si:H layers from optical analysis because (1) except for red light, the incident radiation is absorbed before reaching the n-layer,(2) for typical phosphorous doped n-layers the reflectivity of n- or i-layer/ metal interfaces is about the same, (3) the optical band gap of the n-layer is about the same or slightly smaller than the i-layer. Consequently at longer wavelengths where light is only weakly absorbed in the i-layer, it is also only weakly absorbed in the n-layer and the relative absorption between these two layers is approximately the ratio of there thicknesses[4]. Thus, at most only a few percent of incident light is absorbed in the n-layer.

## 4.1 TCOs

Transparent conductive oxide (TCO) films such as tin oxide ($SnO_2$ ) or indium tin oxide (ITO) or Zinc Oxide (ZnO) have been widely used as transparent electrodes for photovoltaic devices. Particularly in amorphous silicon solar cells tin oxide is known as more suitable material than ITO because of low contamination [17,19] and favourable film surface texture [18,19] but zinc oxide has a strong hydrogen plasma durability during thin film growth[20]. It is also well recognised that the surface morphology of the $SnO_2$ TCOs directly affects the conversion efficiency of a-Si solar cells and consequently the optimisation of the surface morphology of TCO was the most important work on developing the TCO layers used in a- Si solar cells to enhance optical confinement effect [18,19].

TCOs used as a front ohmic contact should be highly transparent and conductive. From the TCO we have used for our work AsahiU, Standard and flat TCO which are tin oxide have a transmittance of around 80% fig(4.1.1, 4.1.2,& 4.1.5) while the ZnO has a transmittance of around 85% fig(4.1.10, 4.1.12, & 4.1.14). This shows that ZnO is more transparent as compared to the other three TCOs. But its application for solar cells is hindered by its blue shift; that is the transmittance drops to zero for $\lambda \leq 370$ nm in the case of ZnO while, it drops to zero for $\lambda \leq$ 320 nm in the case of flat, Asahi U, and standard TCO. Since glass is not transparent for UV light $\lambda \leq 320$ nm the drop in transmittance to zero in the case of flat, Asahi U and standard TCO for $\lambda \leq 320$ nm is not due to absorption within the TCOs rather the glass itself is not transparent. But in the case of ZnO the light with $320\text{nm} < \lambda < 370\text{nm}$ is absorbed by the

ZnO. The light absorbed by ZnO will not contribute to the photovoltaic process, thus the absorbed photons are lost in the TCO.

Optically flat TCO is not a material of choice for solar cells because of its higher reflectance in the visible region fig(4.1.1). It is this region where the a-Si:H solar cell has the highest conversion efficiency.

The area bounded in between the total and specular transmittance has a direct relation to the roughness of the TCO. The larger the area bounded the more rough the TCO is. Thus AsahiU is more rough as compared to the Standard TCO fig(4.1.2 & 4.1.5). The rougher the TCO the more light will be scattered by these rough surfaces thus light will travel a longer path through the solar cell so that the probability of being absorbed there becomes higher. Light is more effectively scattered by AsahiU as compared to standard TCO, and no scattering is observed for flat TCO. Zinc oxide prepared with higher water partial pressure is observed to be more rough as compared to the one prepared with lower water partial pressure fig(4.1.11, 4.1.13,& 4.1.15) by keeping the substrate temperature constant ($330^0$C). Our measurement shows that (20-38) ZnO has got almost the same scattering distribution as Asahi U even though the shape of scattering distributions are different.

The shape of scattering distribution is best described in the range $\theta > 10^0$ by a linear equation for Asahi U which is in agreement with [1] &[21], the square of cosine for standard TCO and polynomial of order 4 for ZnO. It is also observed that ZnO is an angle selective scatterer, it scatters most for larger angles in contrast to Asahi U and standard TCO. The difference in the shape of scattering distribution shows a difference in surface morphology of the TCOs. The scattering distribution for $0 < \theta < 10^0$ is not purely scattered light, it contains both scattered as well as specularly transmitted light.

The natural divergence of the incident beam was $2.8^0$. If we put the TCO on the path of the incident beam the divergence should increase because the light now is embedded by highly refractive index material glass and TCO instead of air. As an example when we write by a white chalk on a dry blackboard the chalk seems bright while if we write by a white chalk on a wet blackboard it is almost invisible. The reason is that in the former case the material between chalk and black board is air but in the latter case the material was the highly refractive index dielectric water.

Blue light is scattered most as compared to green and red light as shown in Fig.(4.1.3&4.1.6). This is so because the roughness of the TCOs are comparable to the wavelength of blue light.

Since the diffused transmittance varies with wavelength $\lambda$ and the scattering angle $\theta$ one can put the measured normalised intensity in a 3-D plot with respect to $\theta$ and $\lambda$, then the measured data points can be connected by a grid structure. This grid structure forms a plane in 3-D, thus the best fit plane to the experimental plane will give $I(\theta, \lambda)$. Thus

$I(\theta,\lambda)=(90-\theta)(a\lambda^2+b\lambda + c)$ fig.(4.1.8) with a maximum deviation of the order of $10^{-7}$ and a, b,& c are of the order of $10^{-11}$, $10^{-8}$, & $10^{-6}$ respectively for Asahi U.

While $I(\theta, \lambda) = (\cos^2 \theta)(a\lambda^2 + b\lambda + c)$ fig.(4.1.9) with a maximum deviation of the order of $10^{-6}$ and a, b, & c are of the order of $10^{-9}$, $10^{-6}$, $10^{-4}$ respectively for standard TCO. The above parameterization was done for $10^0 \leq \theta \leq 90^0$ and for $400nm \leq \lambda \leq 750nm$.

The diffused transmittance calculated by using equation (2.3.9) and the one found by using $T_{total} - T_{specular}$ shows agreement and also the specular transmittance found by using equation (2.3.1) and the one measured by the spectrophotometer shows an agreement.

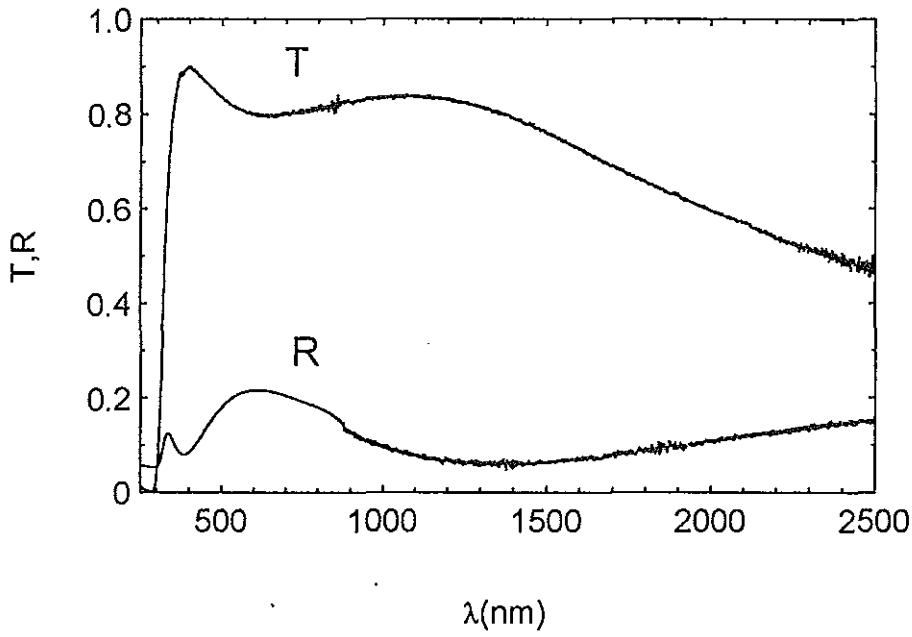


Fig. 4.1.1 Specular reflectance and transmittace of flat TCO

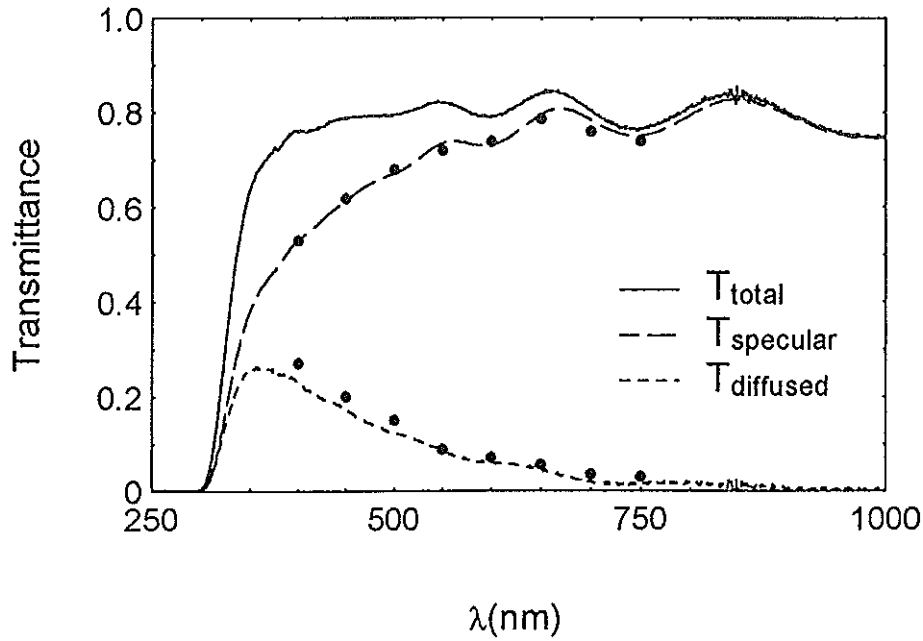


Fig. 4.1.2. Specular ,total&diffused transmittances of Asahi U

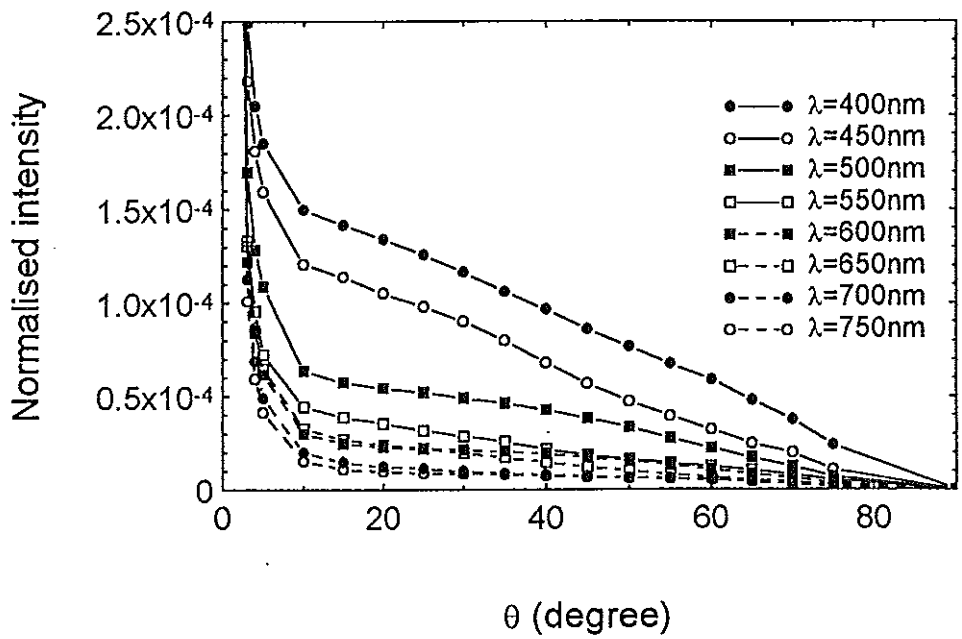


Fig 4.1.3 Angular intensity distribution in transmission for Asahi U

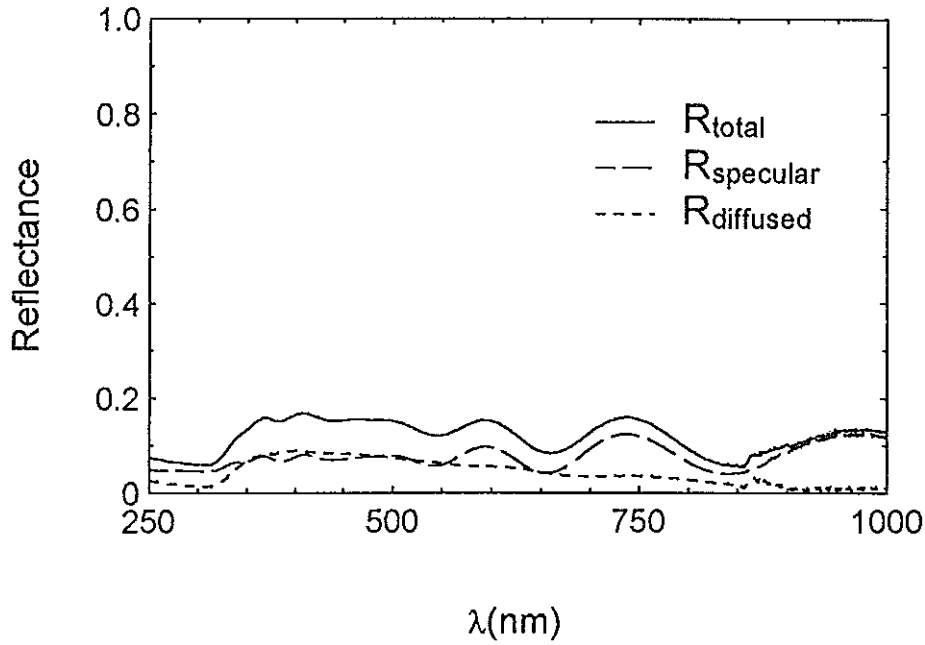


Fig.4.1.4. Specular ,total&diffused reflectances of Asahi U

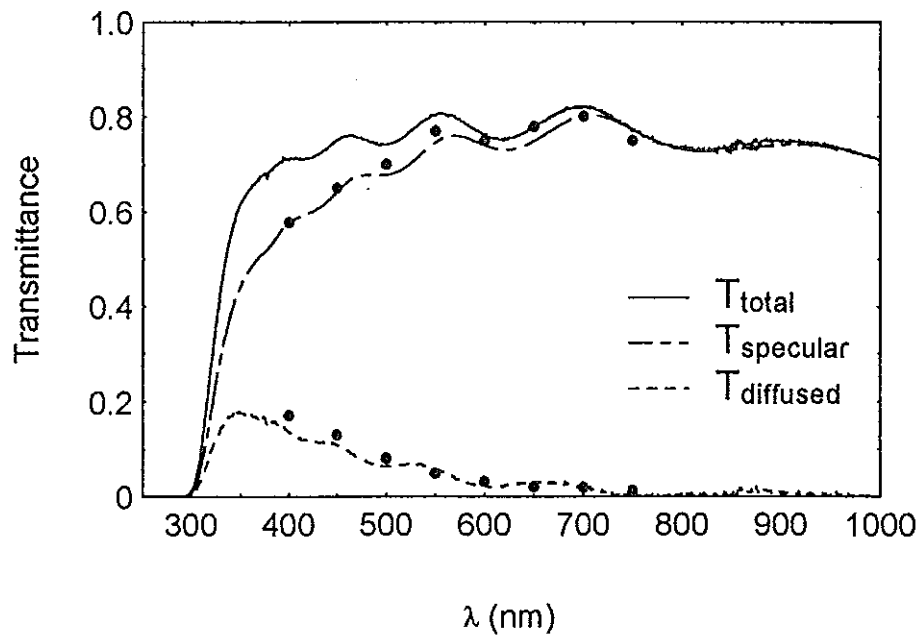


Fig.4.1.5. Specular ,total&diffused transmittances of standard TCO

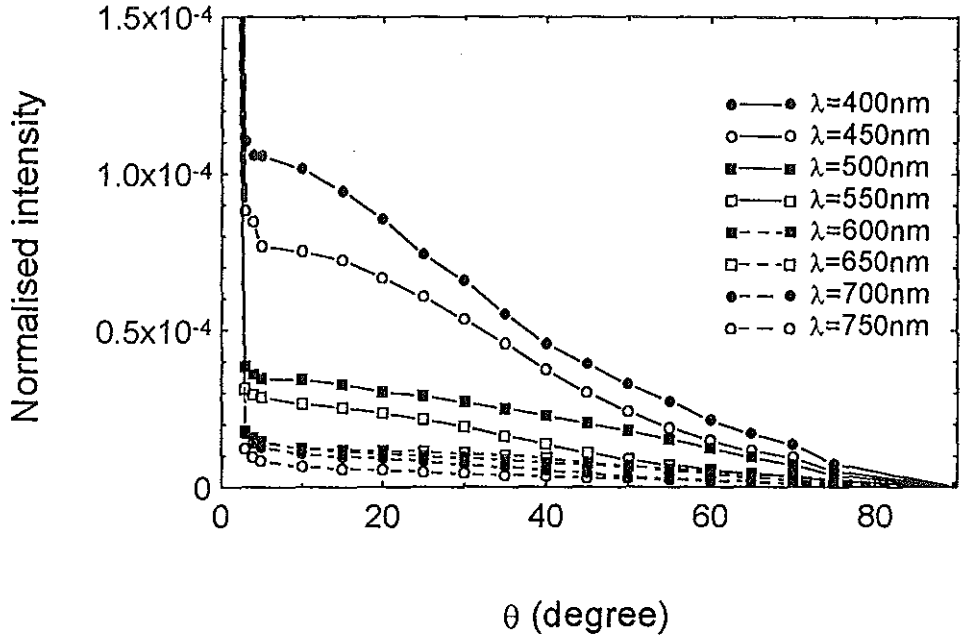


Fig 4.1.6 Angular intensity distribution in transmission for standard TCO

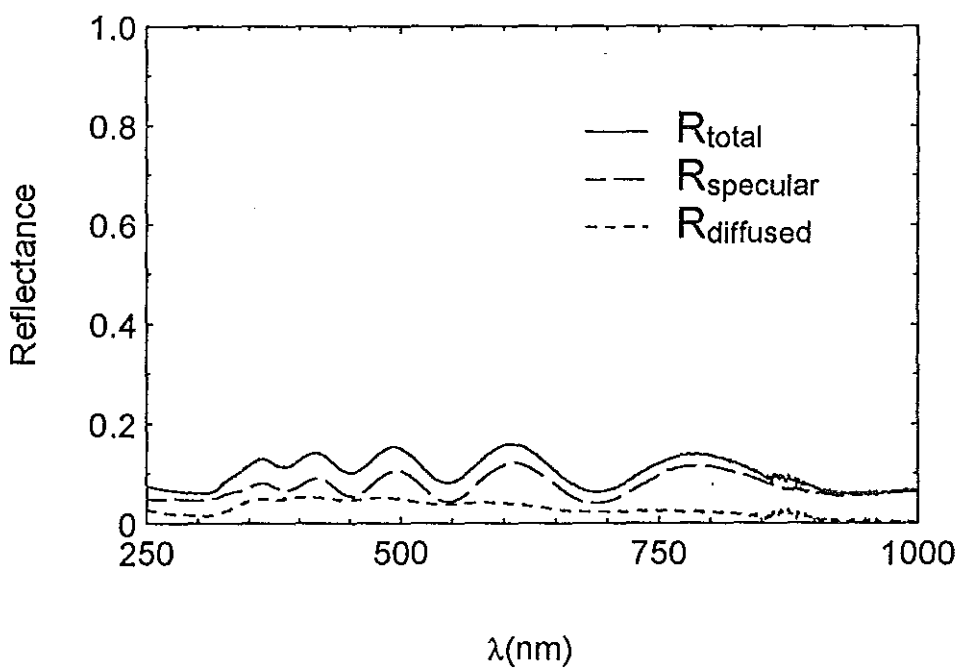


Fig. 4.1.7 Specular ,total&diffused reflectances of standard TCO

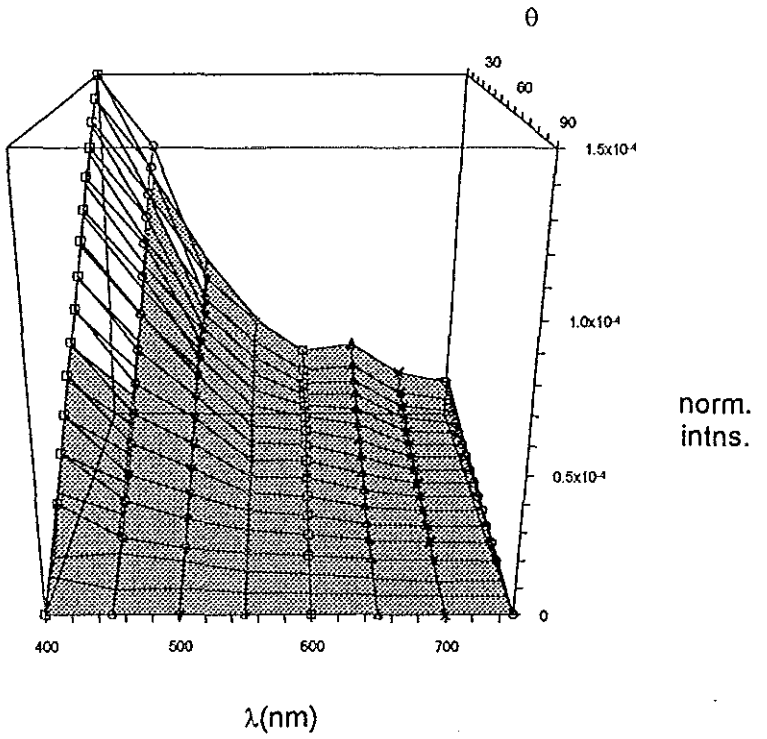


Fig.4.1.8 Three dimensional representaion of normalised intensity as a function of scattering angle θ and wavelength λ for AsahiU. $I(\theta,\lambda) = (90-\theta)(a\lambda^2+b\lambda+c)$.

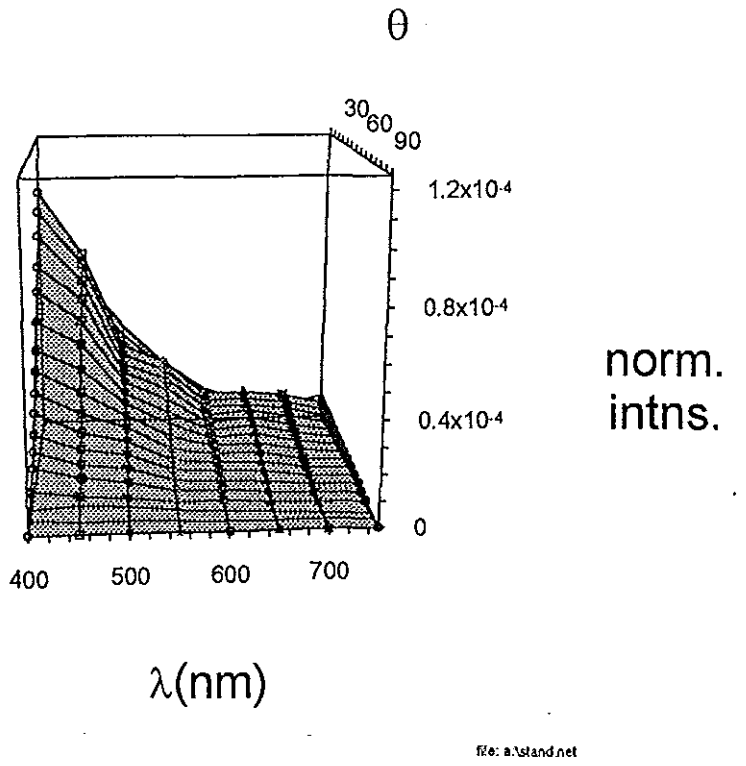


Fig.4.1.9 Three dimensional representaion of normalised intensity as a function of scattering angle θ and wavelength λ for Standard TCO. $I(\theta,\lambda) = \cos^2(\theta)(a\lambda^2+b\lambda+c)$.

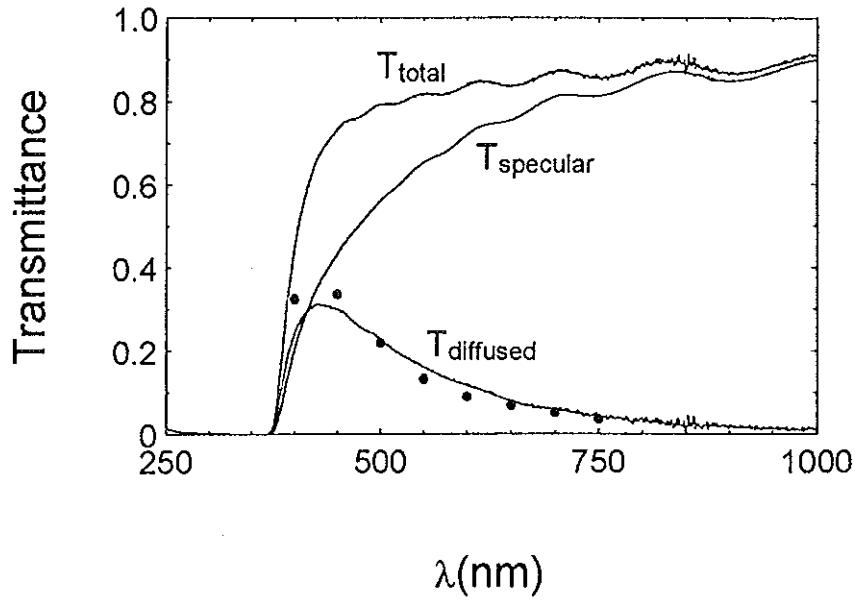


Fig.4.1.10. Specular ,total&diffused transmittances of (20-38)ZnO

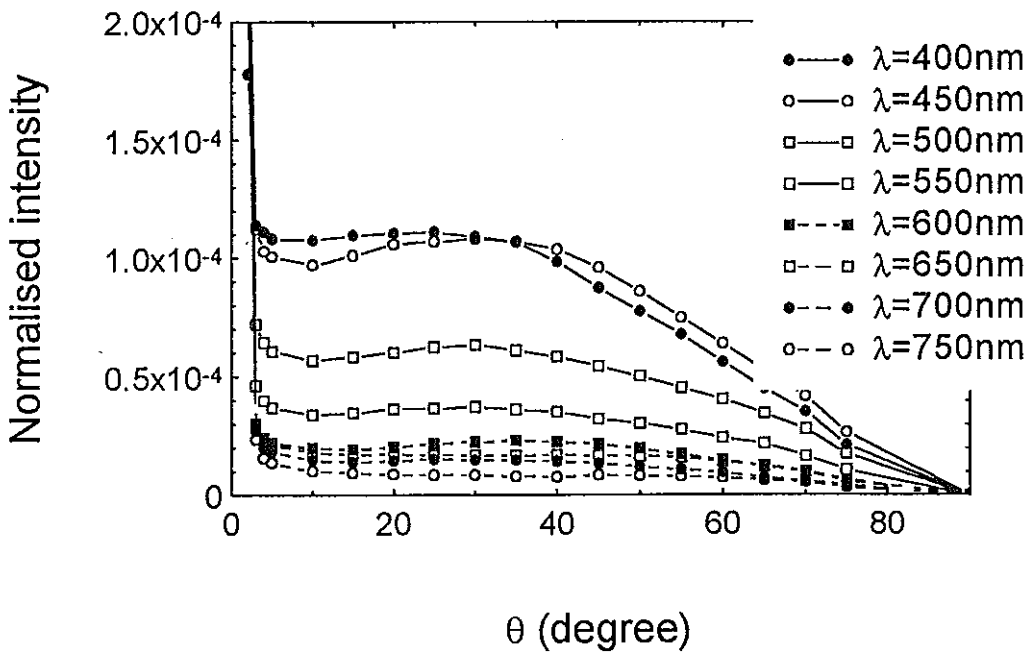


Fig 4.1.11. Angular intensity distribution in transmission for (20-38) ZnO.

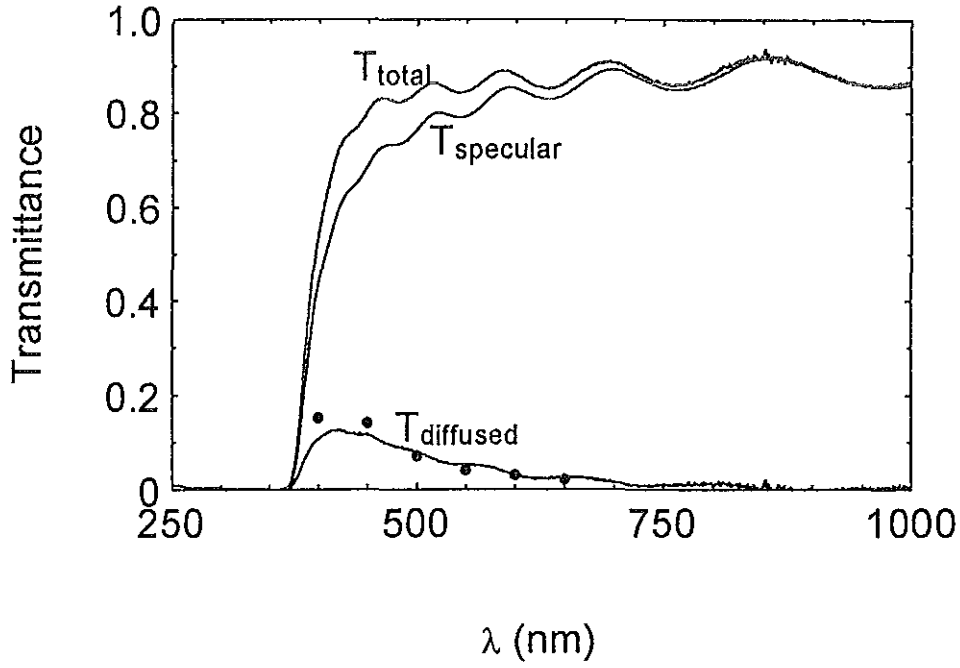


Fig.4.1.12. Specular ,total&diffused transmittances of (22-51)ZnO.

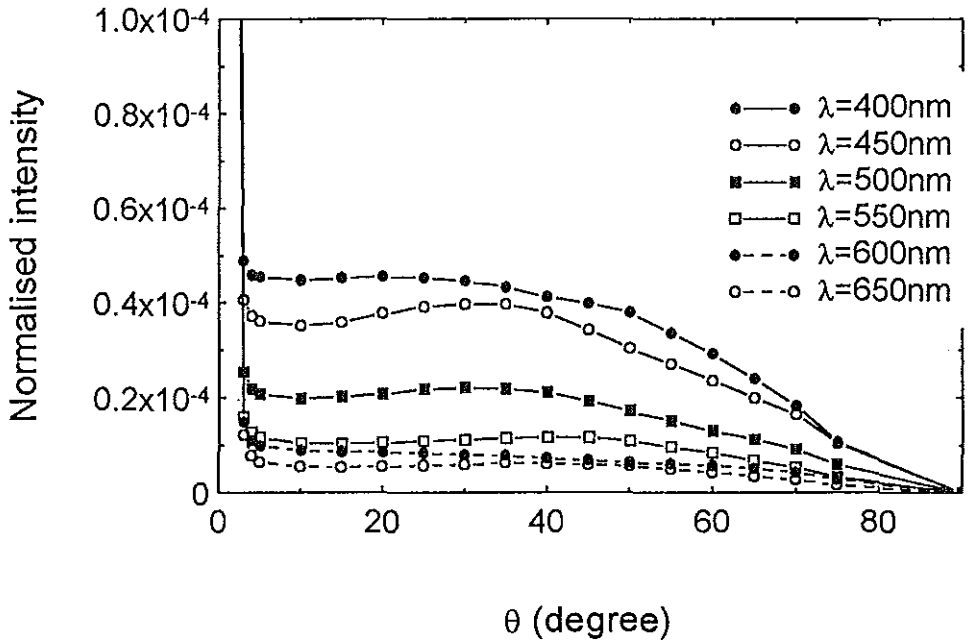


Fig 4.1.13. Angular intensity distribution in transmission for (22-51) ZnO.

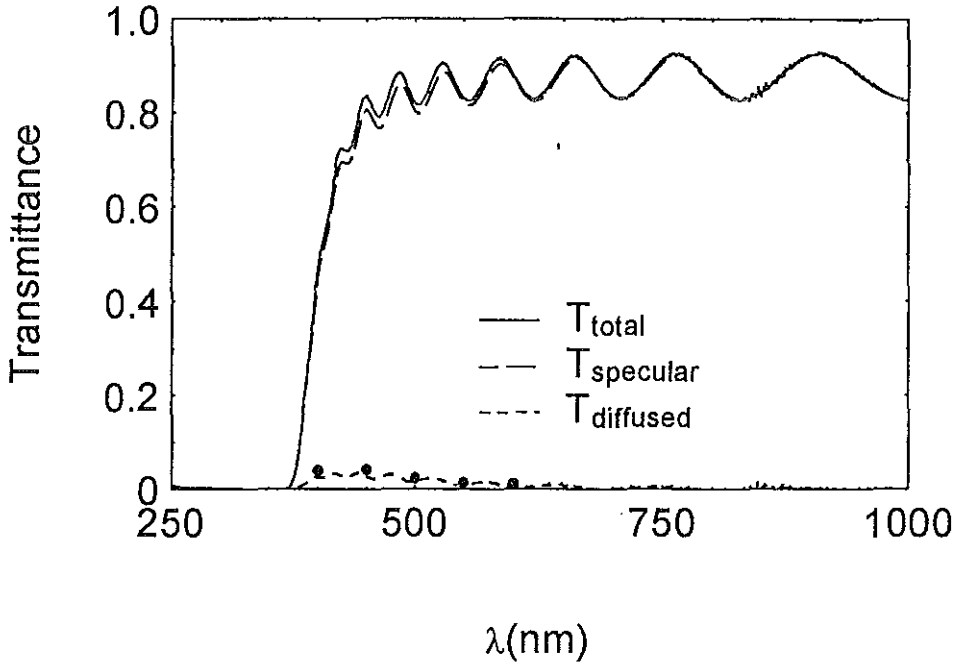


Fig.4.1.14. Specular ,total&diffused transmittances of (22-47)ZnO.

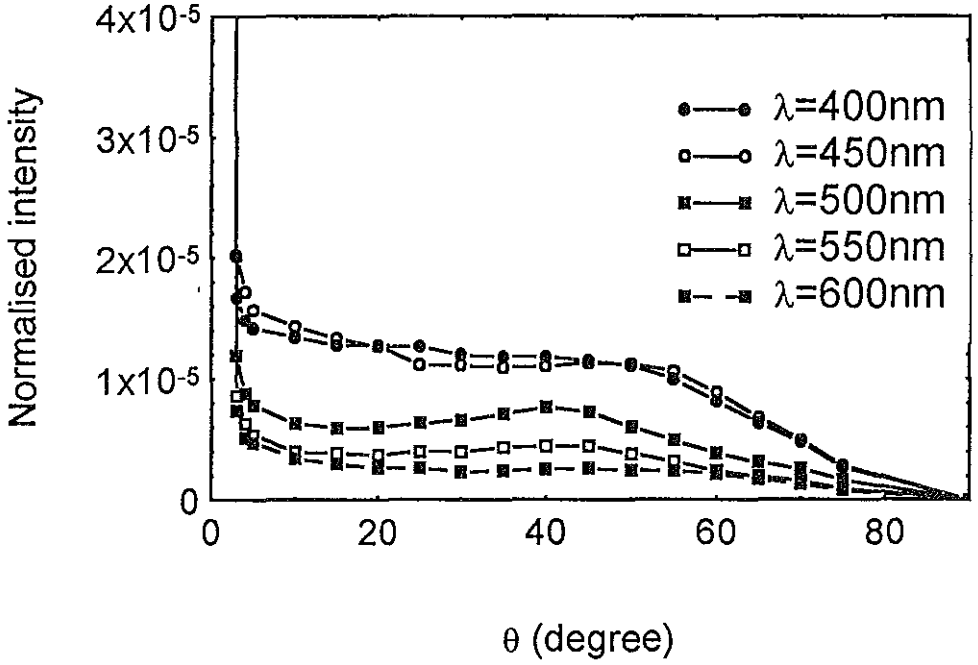


Fig 4.1.15. Angular intensity distribution in transmission for (22-47) ZnO.

## 4.2 TCOs /P-Layer (15 nm)

The absorption losses in the p-layer are severe for short wavelength light. It could be significantly reduced by increasing the optical gap and decreasing the thickness of the p-layer [22]. The optical gap of the p-layer can be increased by introduction of methane.

According to our experimental results the transmittances are significantly reduced for short wavelength (blue light) but no much deviation was observed for long wavelength light. The reflectances are very slightly increased for short wavelengths but no change was observed for higher wavelengths fig.(4.2.4 & 4.2.6). The scattering distributions are also significantly reduced for short wavelength light fig(4.2.3 & 4.2.6). The reduction in the scattering distribution is due to light losses. There could be at least four reasons for these losses viz.

a. Most of the lost light is absorbed by the p-layer, which is not desired to be lost there.
b. Part of the lost light is reflected back at the TCO / p-layer interface.
c. Part of the lost light may be due to loss of coherence (due to interference between incident and reflected light).
d. The roughness of the scattering surface may be reduced with the p-layer deposition.

The shape of the scattering distribution changes for the Asahi U sample with additional p-layer deposition while it is not changed for standard TCO. The amount of the scattering distribution decreased for both TCOs fig(4.2.3 & 4.2.6). The shape of the scattering distribution is best described by the square of cosine with respect to the scattering angle $\theta$ for both TCOs. This shows that the surface morphology of Asahi U is more affected by the p-layer deposition than standard TCO.

Even with an additional p-layer deposition Asahi U scatters most as compared to standard TCO, which makes it a suitable front window material for solar cells. The diffused transmittance calculated from the scattering distribution measurement shows an agreement with the one measured by using spectrophotometer fig(4.2.2 & 4.2.5).

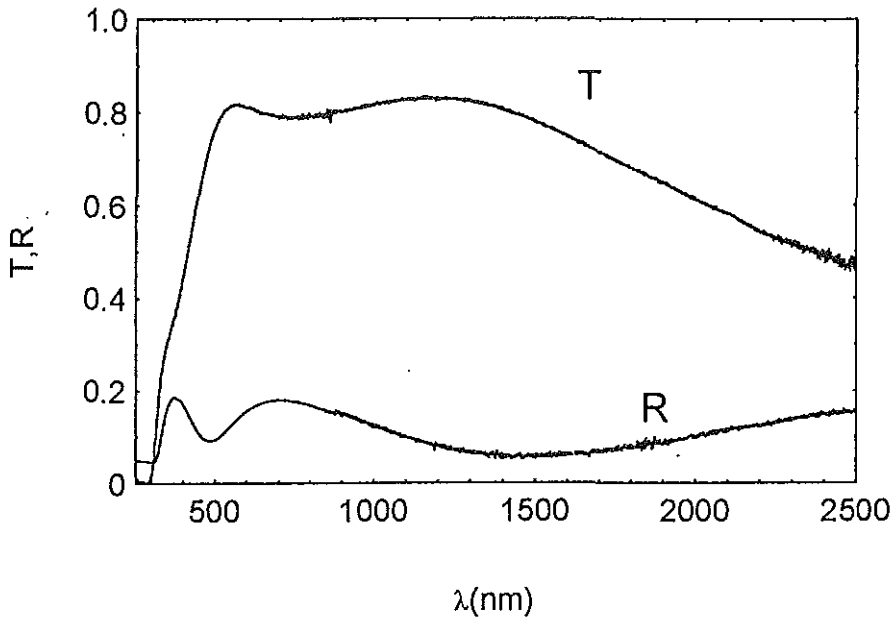


Fig. 4.2.1. Specular reflectance & transmittance of flat TCO / p-layer(d=15nm)

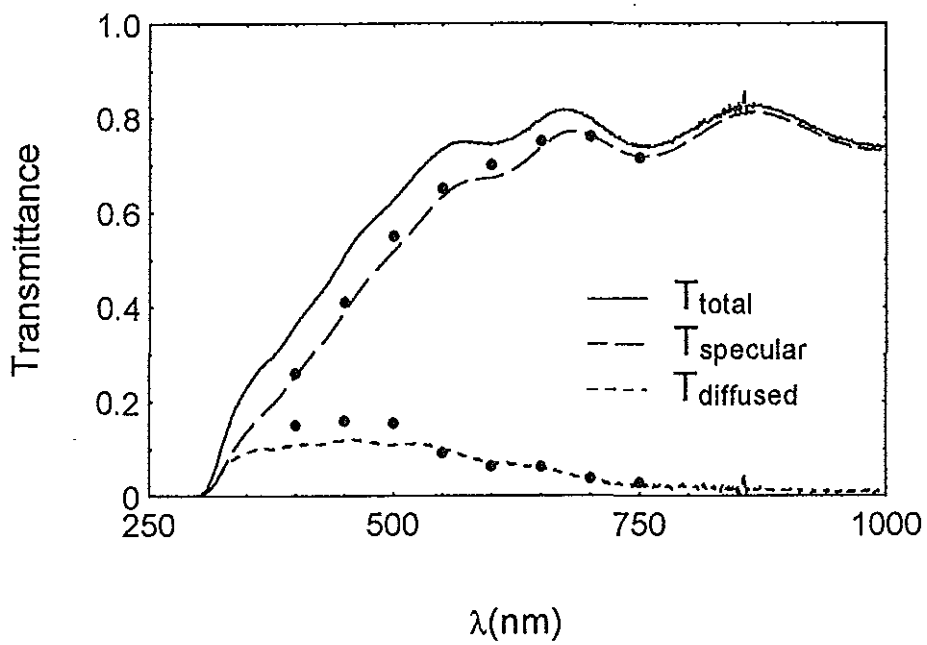


Fig. 4.2.2 Specular , total & diffused transmittances of Asahi U / p-layer (15nm)

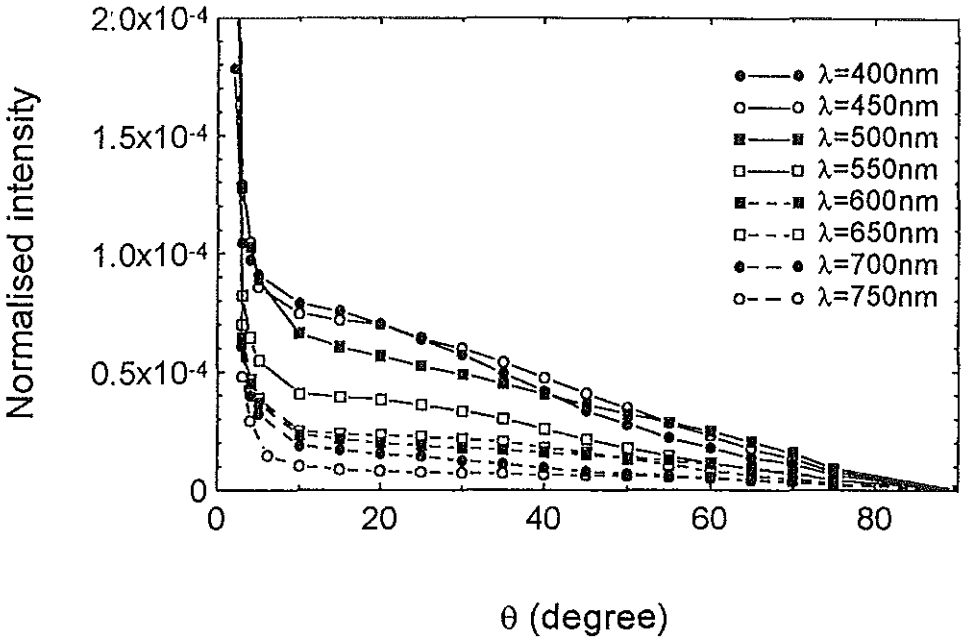


Fig. 4.2.3 Angular intensity ditribution in transmission for Asahi U / p-layer (15nm)

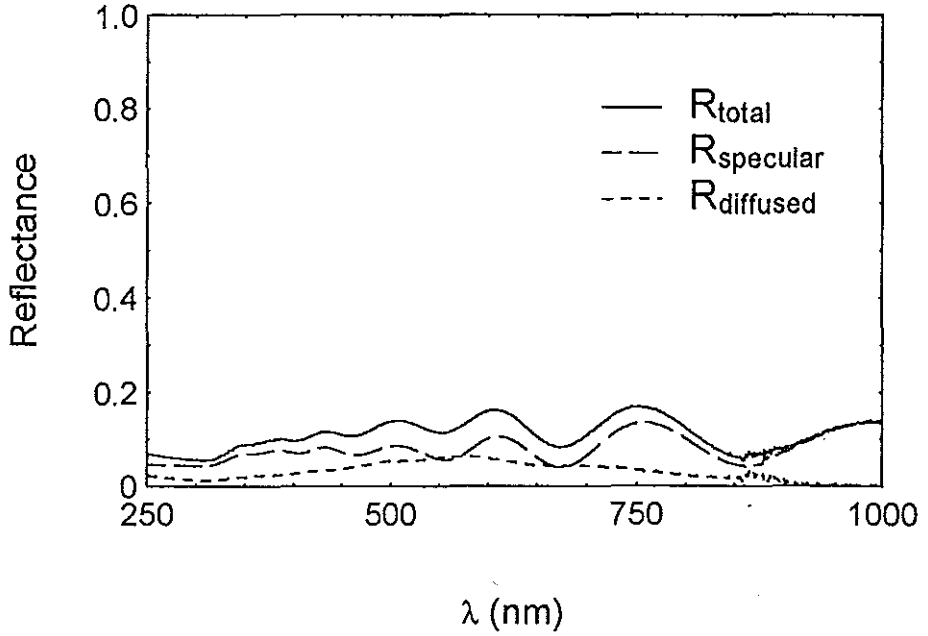


Fig. 4.2.4 Specular , total & diffused reflectances of Asahi U / p-layer (15nm)

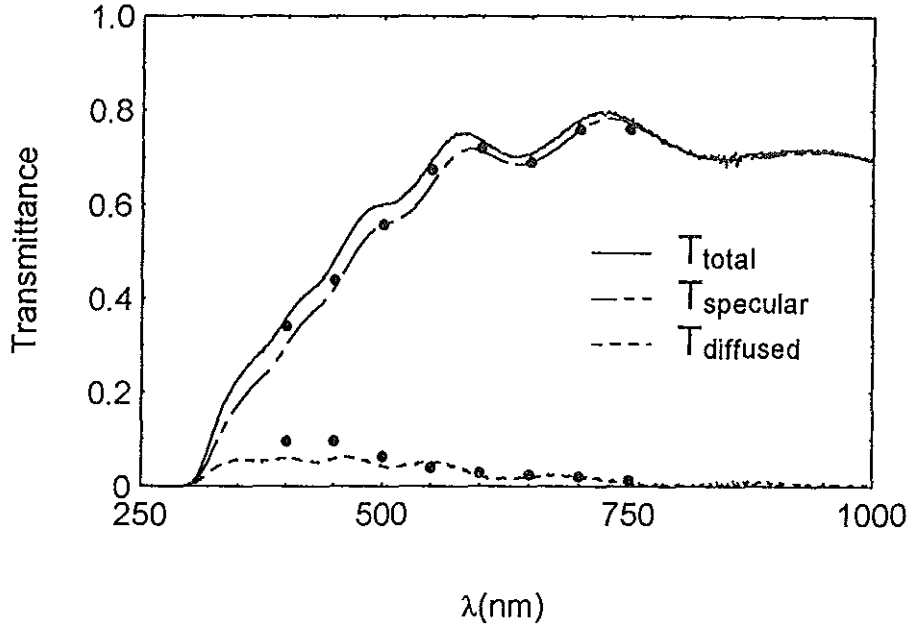


Fig. 4.2.5 Specular , total & diffused Transmitances of standard TCO / p-layer (15nm)

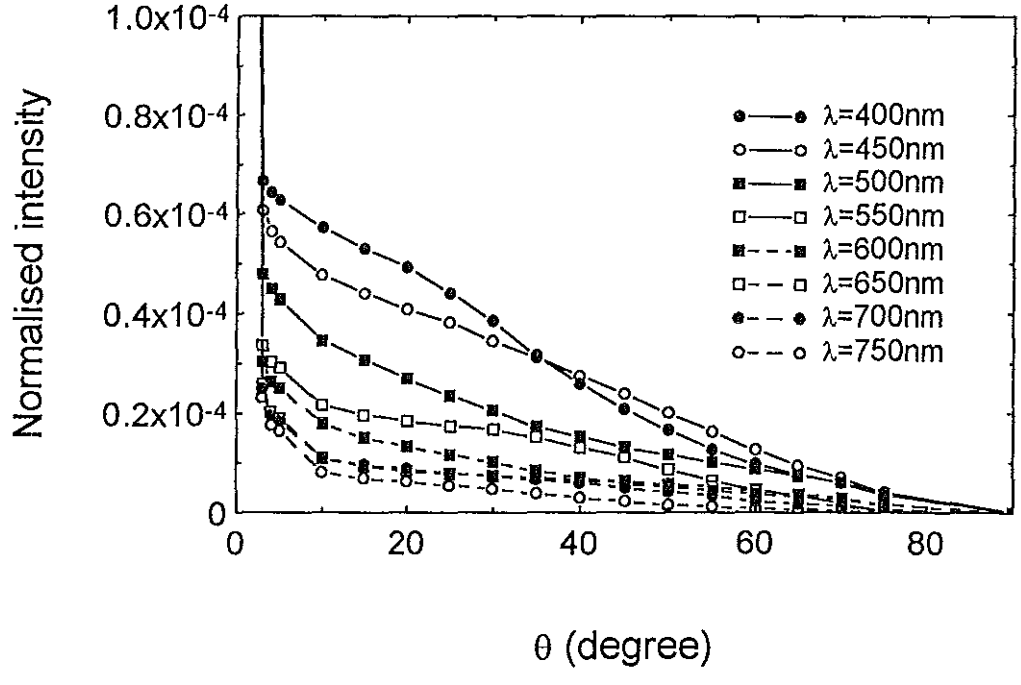


Fig. 4.2.6 Angular intensity distribution in transmission for standard TCO / p-layer (15nm )

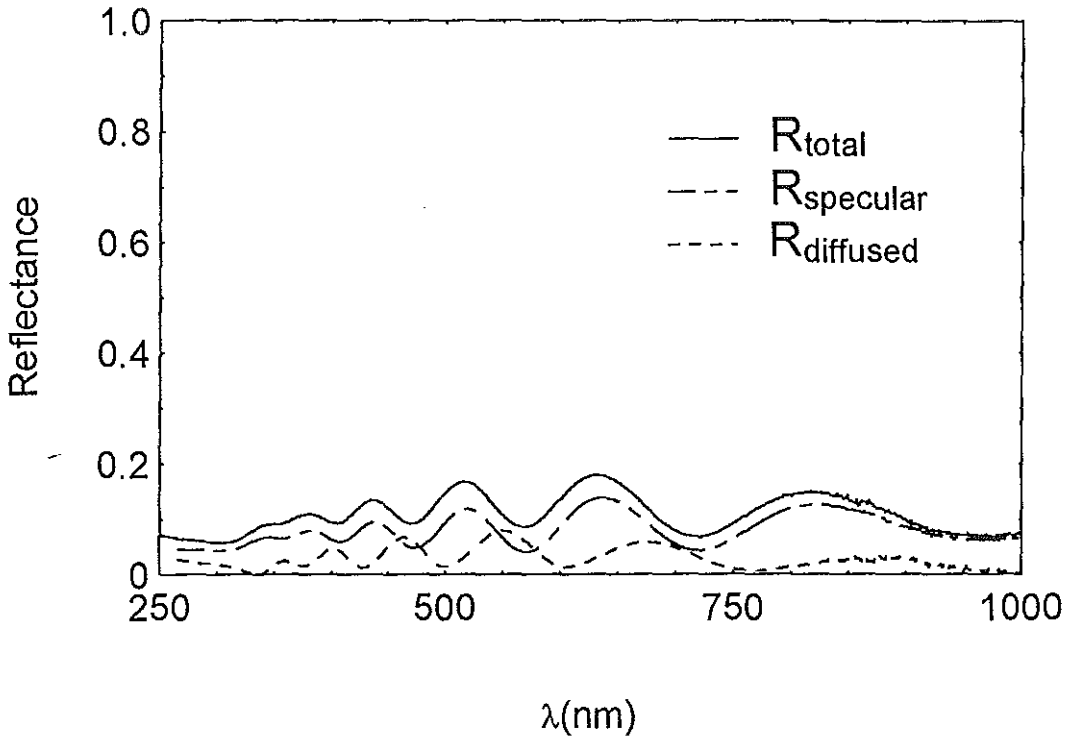


Fig. 4.2.7 Specular , total & diffused reflectances of standard TCO / p-layer (15nm)

## 4.3 TCOs /P-layer (15 nm) / i-layer (50 nm)

Studying the optical properties of thin film layers and layer stacks is very important since it reflects the real situation in a-Si:H solar cells.

Fig. 4.3.1 to Fig. 4.3.7 show the optical behaviour of the three kinds of TCOs with additional 15nm thick p-layer and an additional 50 nm thick i-layer. The transmittance drops to zero for wavelengths $\lambda \leq 390$ nm and decreases strongly for $\lambda > 390$ nm for flat TCO with p- and i- layers (Fig 4.3.1). This is not because all the light is absorbed by the 50 nm i-layer rather the reflectance increases considerably. Even for higher wavelengths the reflectance is greater than the transmittance.

The transmittance drops to zero at $\lambda \leq 390$ nm and decreases strongly for $\lambda$>390nm for Asahi U with p- and i-layers compared to the case of Asahi U without i-layer Fig.(4.3.2 & 4.2.2). This is so because light with $\lambda < 390$ nm is completely absorbed and a decrease in transmittance up to $\lambda = 600$ nm is also due to absorption by the i-layer since no increase in reflectance was observed. While the decrease in transmittance for $\lambda > 600$nm is not due to pure absorption since the reflectance increases considerably (compare fig(4.3.4) to fig(4.2.4)). This is so because the absorption of red light by a-Si:H layers is very small. The argument stated for Asahi U also holds for standard TCO with p-layer(15nm) and i-layer(50nm) except that Asahi U with layers absorbs more in the green and red light region. This is so because of its higher scattering ability.

Even with p- and i-layers Asahi U scatters most as compared to standard TCO. The shape of the scattering distribution can be best described by a polynomial of the second order for all wavelengths measured and for both TCOs.

The normalised scattered intensity now is in the reverse order. Short wave length light scattered less as compared to long wavelength light. The reason is that short wave length light is strongly absorbed by the amorphous layers.

In the red light region the diffused transmittance of TCOs with p- and i-layer is large as compared to TCOs with p-layer and pure TCOs fig(4.3.2 & 4.3.5). The reason is that since red light is not strongly absorbed by a-Si:H layers those light reflected back at i-layer/air interface will again be reflected back at p-/i-layer, TCO/ p-layer, TCO/glass and air/glass interfaces so as to increase the diffused transmittance (multiple reflection effect). The spectral fringes on reflectance and transmittance curves of TCOs and TCOs with layer stacks are due to the thickness and refractive indices of the films. The periodicity of the fringes is inversely proportional to the product of the thickness and refractive indices of the films. Thickness of the films do not change with wavelength. However, refractive indices of the films are wavelength

dependent. Refractive indices of films are decreasing with increasing wavelength [23,4,24]. The halfwidth of the spectral fringes of the transmittance and reflectance curves become broader with increasing wavelength

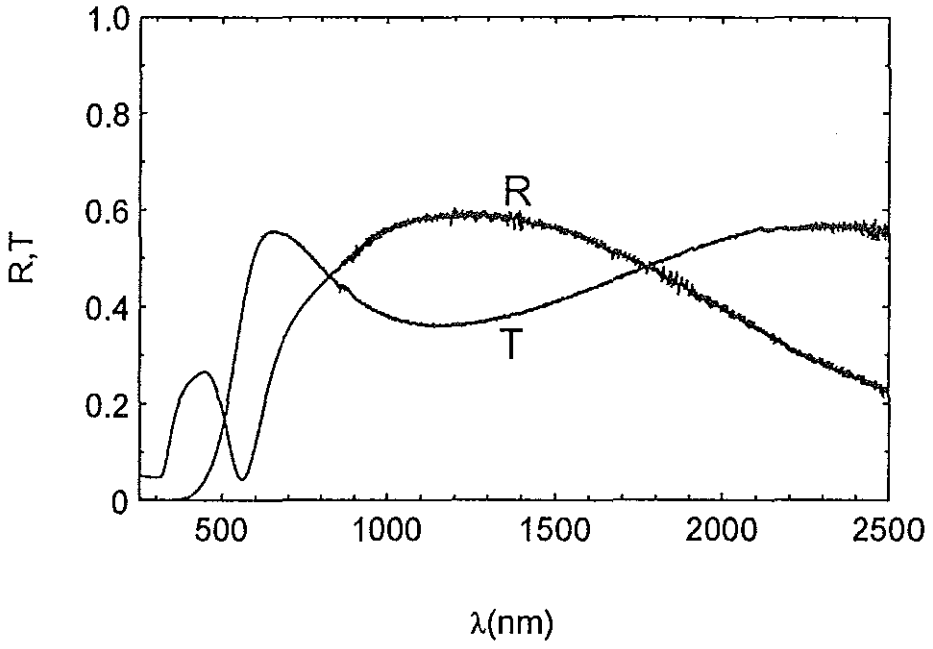


Fig. 4.3.1 Specular reflectance & transmittance of flat TCO / p-layer (15nm) /i-layer (50nm)

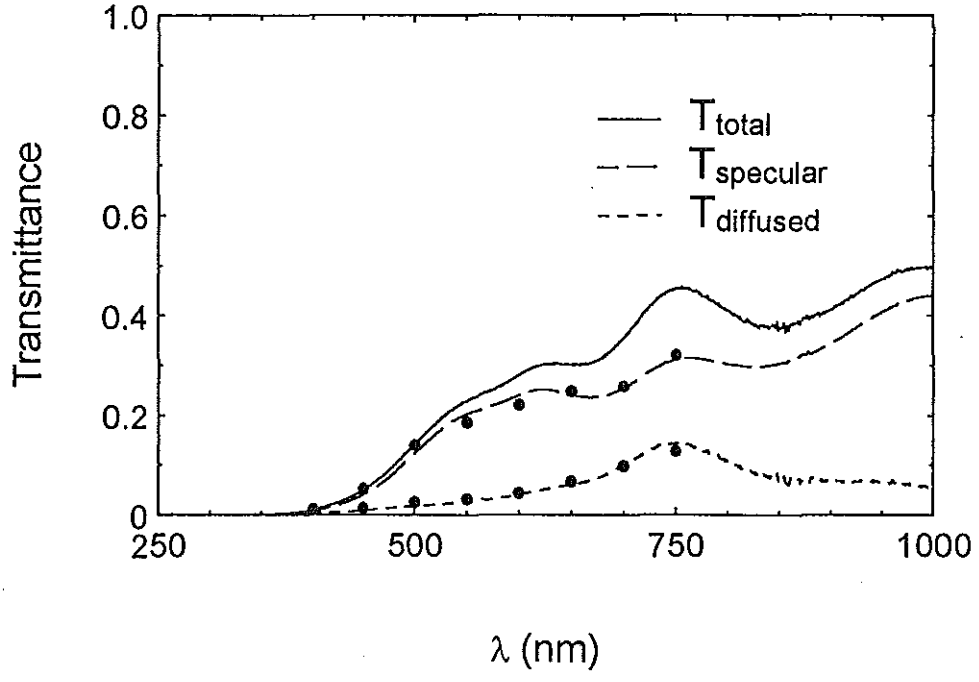


Fig. 4.3.2 Specular reflectance & transmittance of AsahiU / p-layer (15nm) /i-layer (50nm)

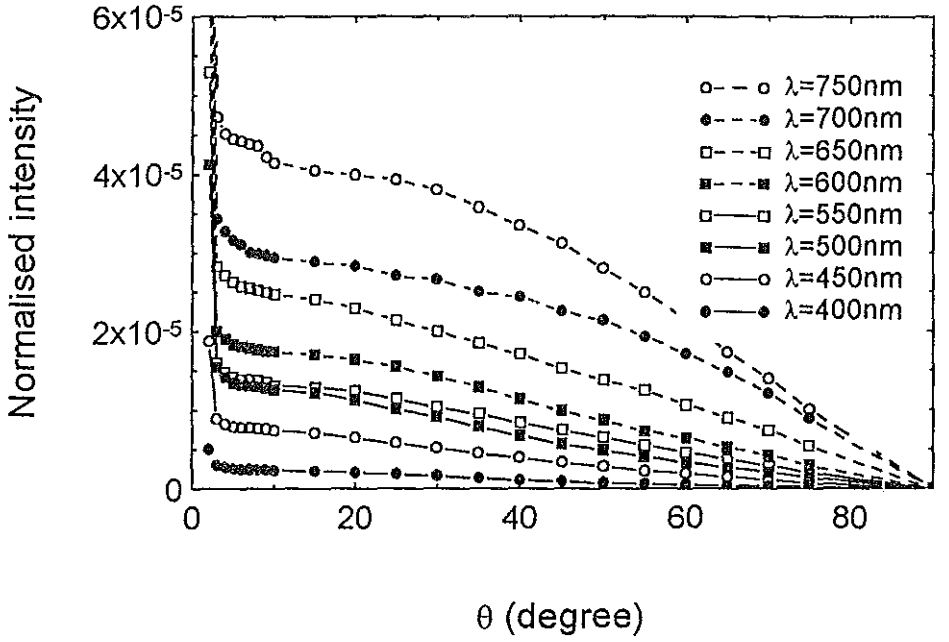


Fig. 4.3.3 Angular intensity distribution in transmission for Asahi U / p-layer (15nm) / i-layer (50nm)

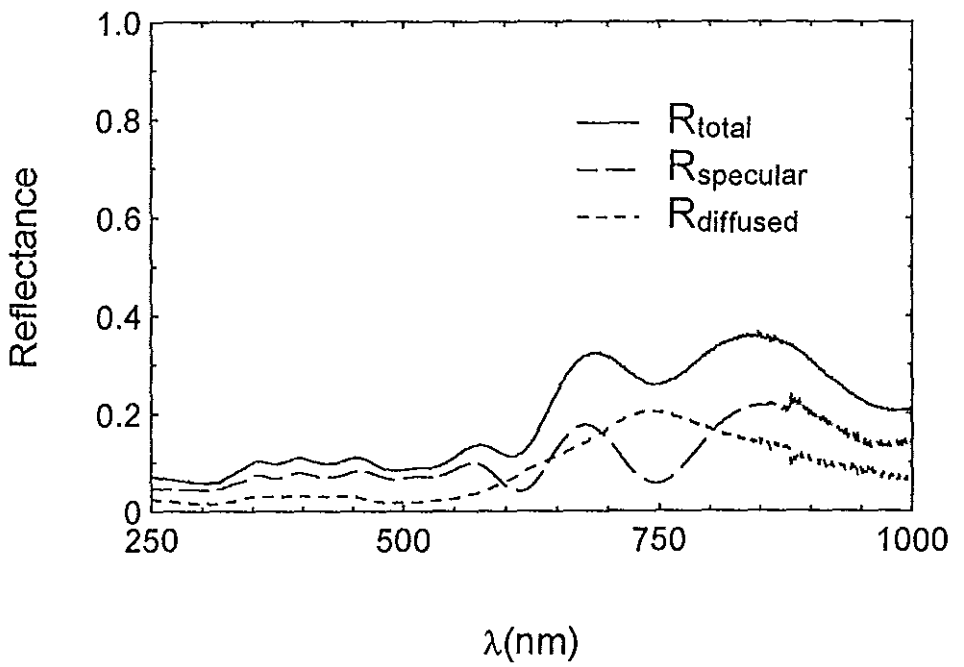


Fig.4.3.4 Specular , total & diffused reflectances of Asahi U / p-layer (15nm) / i-layer (50nm)

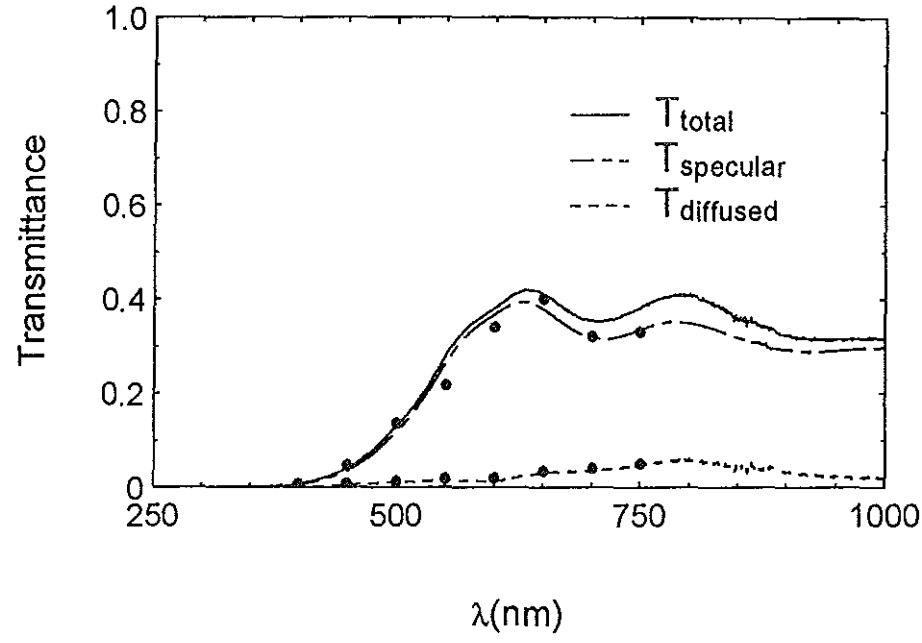


Fig.4.3.5 Specular , total & diffused transmittances of standard TCO / p-layer (15nm) / i-layer (50nm)

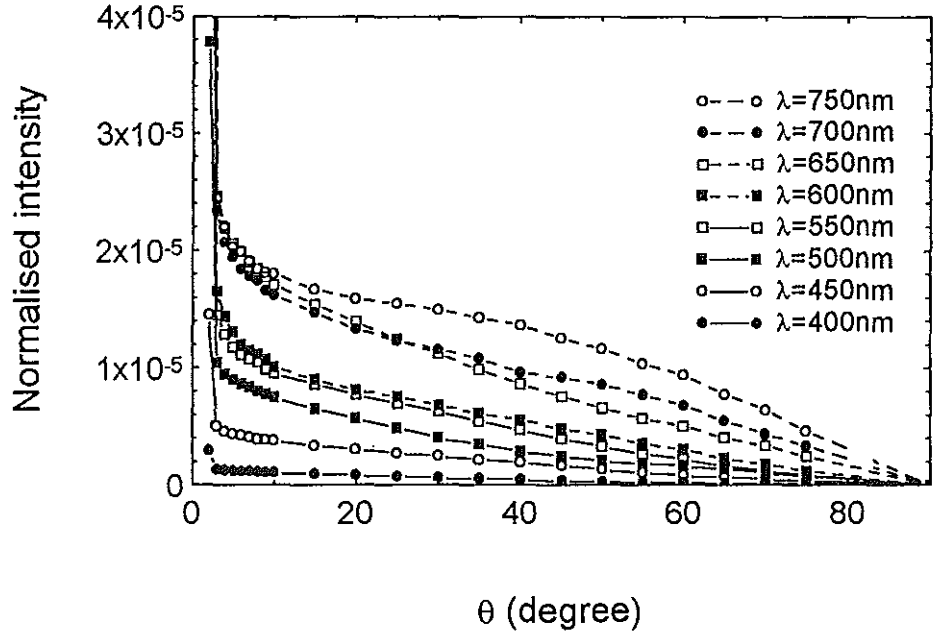


Fig. 4.3.6 Angular intensity distribution in transmission for standard TCO / p-layer (15nm) / i-layer (50nm)

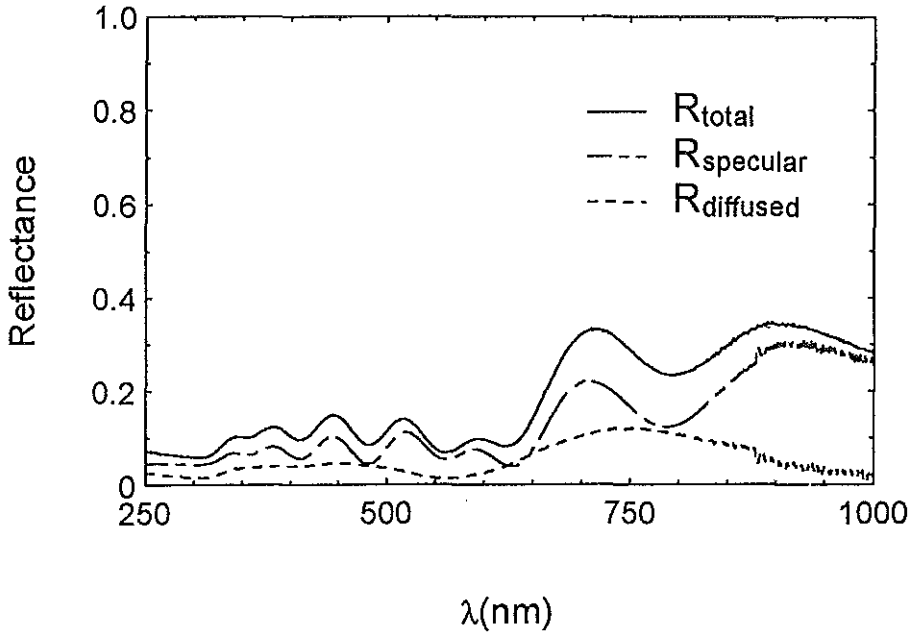


Fig.4.3.7 Specular , total & diffused reflectances of standard TCO / p-layer (15nm) / i-layer (50nm)

## 4.4. TCOs /P-layer (15 nm)/i-layer (380 nm)

In this section we to see the effect of the thickness of the i-layer on the optical absorption, transmittance and reflectance. This section deal a realistic i-layer thickness while in section 4.3 we use 50 nm i-layer just for index matching purpose. Fig. 4.4.1 to Fig. 4.4.7 shows the optical behaviour of the three kinds of TCOs with p-layers (15 nm) and i-layers (380 nm). Light with wavelength $\lambda \leq 500$ nm is strongly absorbed in the thick i-layer with a small increase of reflectance by flat TCO Fig. (4.4.1) , while the light with wavelength greater than 500 nm is not much absorbed since the reflectance is getting large. The spectral fringes on R and T curves become narrow due to the increase in the thickness of i-layer.

The transmittance drops to zero at wavelength $\lambda \approx 550$ nm and decreases considerably for $\lambda > 550$ nm for Asahi U with p-layer (15 nm) and i-layer (380 nm) Fig.(4.4.2). The reason is that light with wavelength less than 650 nm is strongly absorbed by the thick i-layer with a reflectance of around 10%. This shows that blue and green light is effectively absorbed and red light with wavelength less than 650 nm is strongly absorbed by the thick i-layer. The transmittance drops to zero at wavelength $\lambda \approx 530$ nm and decreases considerably for $\lambda >$ 530nm for the standard TCO with p-layer (15 nm) and i-layer (380 nm) Fig.(4.4.5); with the same reason as Asahi U with layers. Asahi U with layers absorbs most as compared to standard TCO with layers. In both TCOs most of the absorption takes place within the intrinsic layer which is the layer of interest for light to be absorbed.

Asahi U with p-layer and thick i-layer scatters most as compared to standard TCO with the p-and i-layers Fig.4.4.3. and Fig.4.4.6. But the shape of scattering distribution could be approximated by cosine of scattering angle $\theta$. This shows that both TCOs with 15nm p-layer and 380 nm i-layer tend to behave as a Lambertian scatterer $I = I_o \cos(\theta)$. The scattering ability increases with wavelength $\lambda$ by the same reason as stated in section 4.3. We have also observed that the maxima of the diffused transmittance shifts to higher wavelength with increasing the thickness of the i-layer.

We restricted our study to the visible region because in this region amorphous hydrogenated silicon has the highest conversion efficiency. Therefore within the visible region Asahi U with layer stacks absorbs and scatters most as compared to standard and flat TCO with their layer stacks. Thus from optical point of view AsahiU is considered to be a suitable material for a-Si:H solar cells.

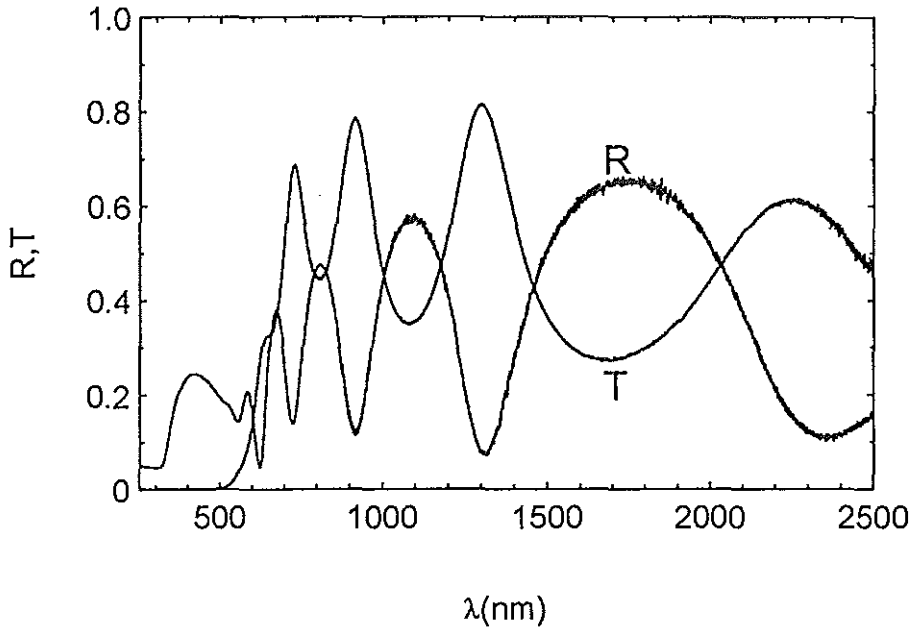


Fig. 4.4.1 Specular reflectance & transmittance of flat TCO / p-layer (15nm) / i-layer (380nm)

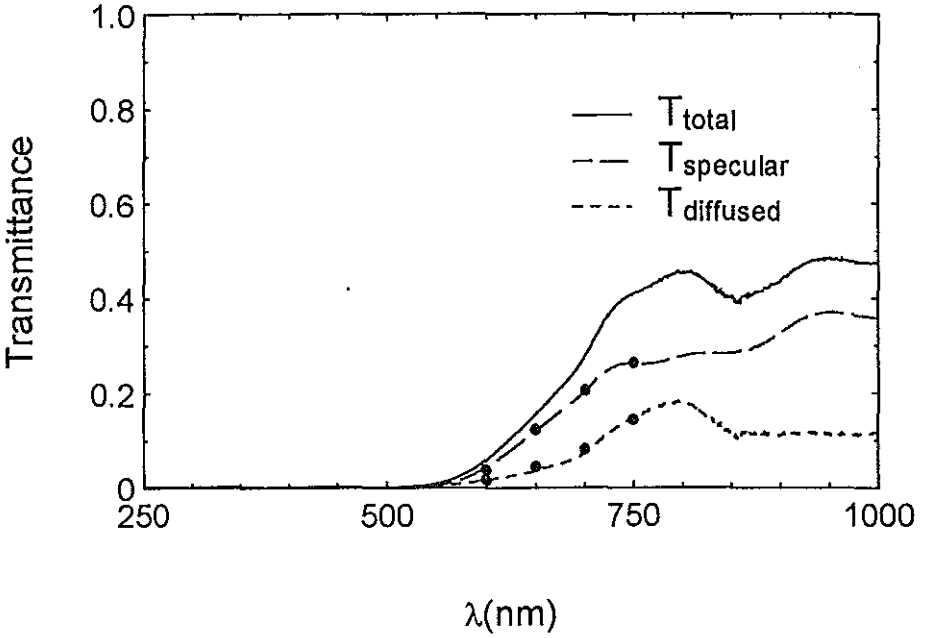


Fig. 4.4.2 Specular , total & diffused transmittances of Asahi U /p-layer (15nm) / i-layer (380nm)

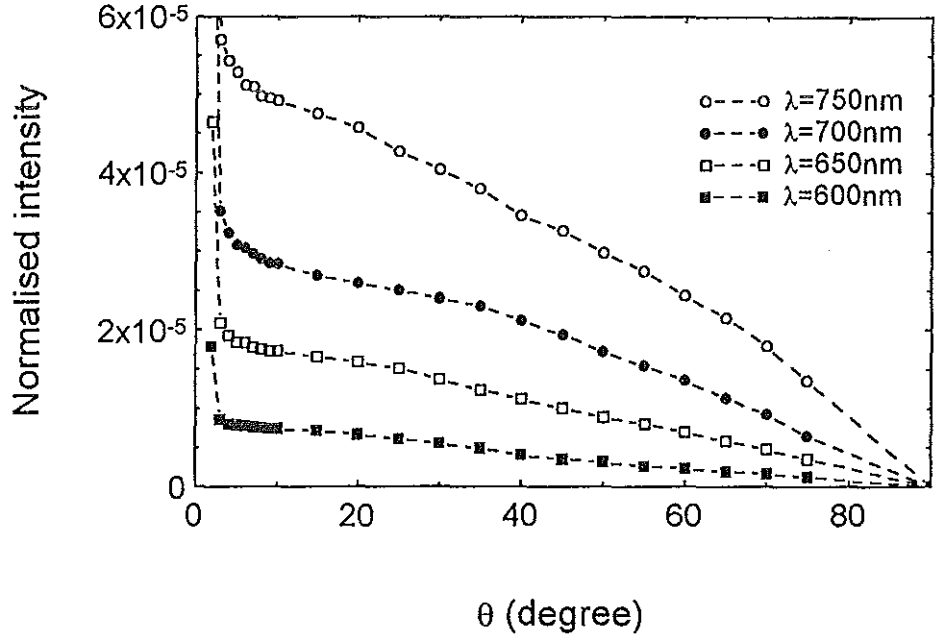


Fig.4.4.3 Angular intensity distribution in transmission for Asahi U /p-layer (15nm) / i-layer (380nm)

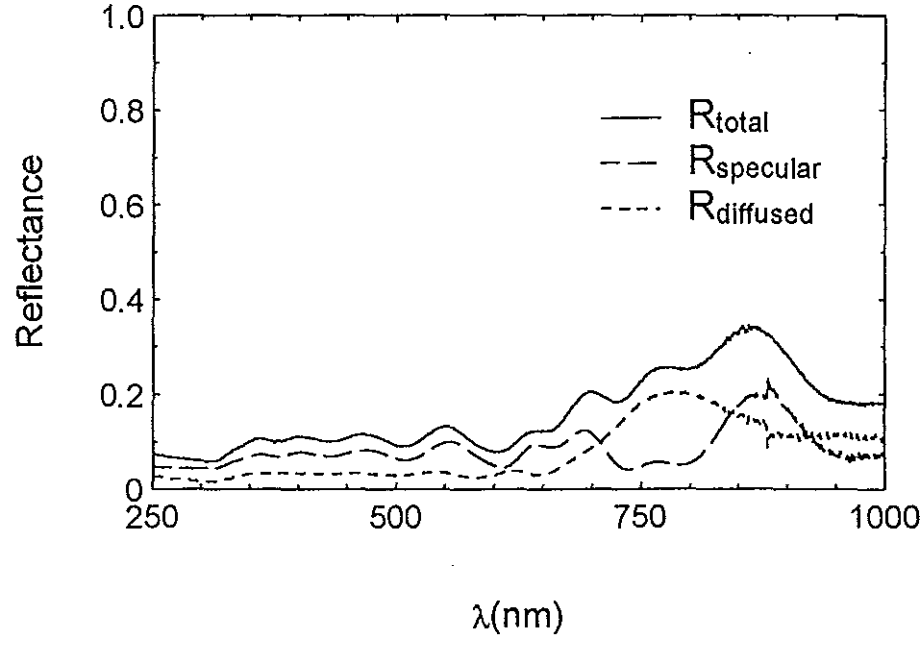


Fig. 4.4.4 Specular , total & diffused reflectances of Asahi U /p-layer (15nm) / i-layer (380nm)

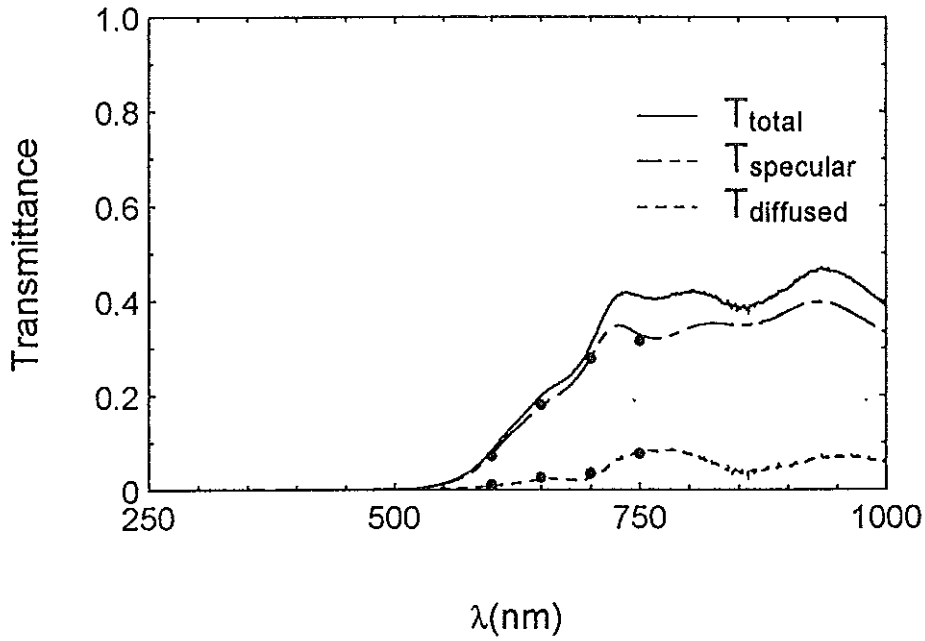


Fig. 4.4.5 Specular , total & diffused transmittances of standard TCO /p-layer (15nm) / i-layer (380nm)

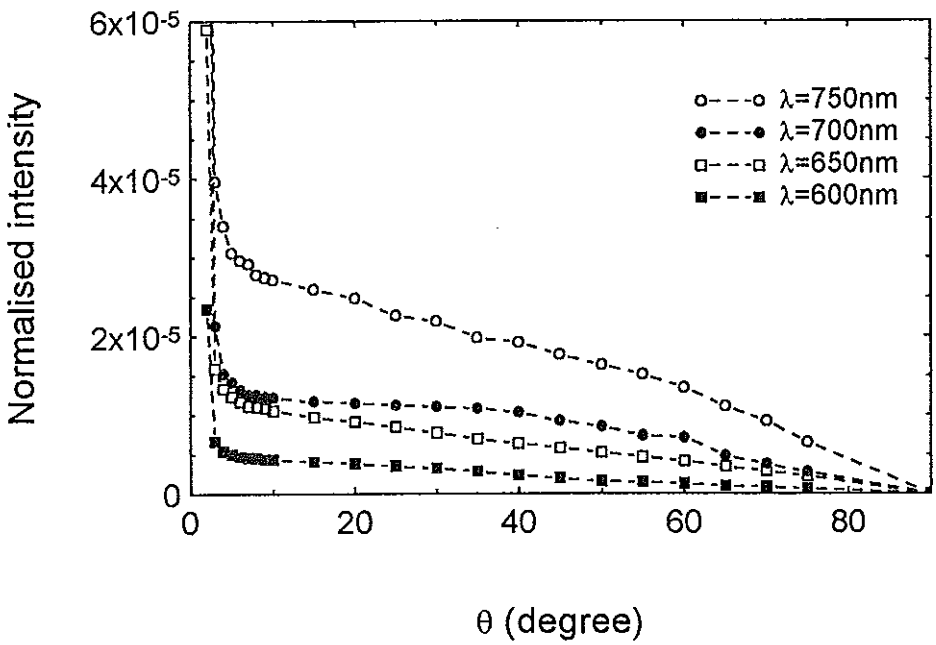


Fig.4.4.6 Angular intensity distribution in transmission for Standard TCO / p-layer (15nm) / i-layer (380nm)

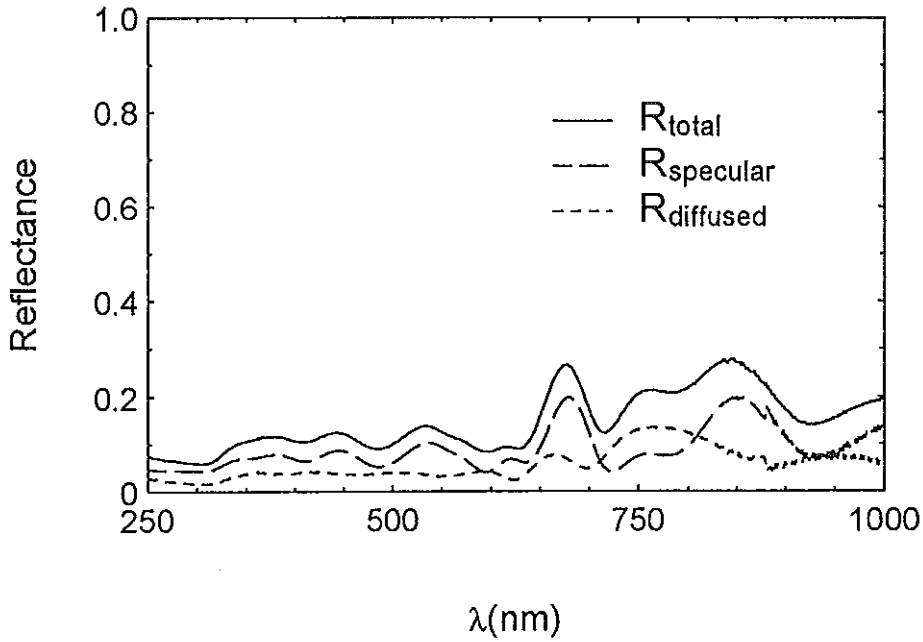


Fig. 4.4.7 Specular , total & diffused reflectances of standard TCO /p-layer (15nm) / i-layer (380nm)

# 5. Conclusion

The aim of this work was to measure the scattering distribution of different kinds of TCOs with and without layer stacks, and to suggest which TCO is best for solar cell application from an optical point of view. Scattering distribution of various TCOs with and with out their layer stacks have been measured. The shape of the scattering distribution was observed to be linear for Asahi U which is in a good agreement with[1,21], square of cosine of θ for Standard TCO, polynomial of order 4 for ZnO; square of cosine of θ for both Asahi U & Standard TCO/p-layer(15nm); polynomial of order 2 for both Asahi U & Standard TCO/p-layer(15nm)/ i-layer(50nm); and cosine of θ for both Asahi U & Standard TCO/p-layer(15nm)/ i-layer(380nm). In all cases Asahi U scatters most as compared to the rest even with its layer stacks . Therefore Asahi U can be considered as the best TCO for solar cell application.

TCOs and TCOs/p-layer stacks absorb very small amount of the incident photons, while TCOs/p-layer/i-layer absorbs most of the incident photons.This means that most of the incident photons are absorbed by the i-layer. This is so because i-layer has a higher absorption coefficient and is also the layer where light needed to be absorbed.

Further work could be done to relate the scattering distribution with the microstructure of the thin film rough layers and layer stacks. Even though, we have measured the scattering distribution for rough layer stacks, it has to be transformed in to buried layers because the scattering distribution on the buried manifests the real situation in solar cell.

## References


1. Tao G. Optical Modelling and Characterisation of Hydrogenated Amorphous Silicon, Delft University press, 1994, 8-34.
2. Yang J et al. 25th IEEE PVSC, USA ,1996.
3. Bennet J.M, and Mattsson, L. Introduction to Surface Roughness and Scattering, Optical Society of America, 1989, 35-56.
4. Ellis F.B. and Delahoy A.E. Reprinted from solar energy materials, 1985, 1074-1087.
5. Winz K. et al. 25th IEEE PVSC USA 1996.
6. Tao G. et al. Verhoging van het Rendement Van amorf Silicium Zonnecellen door middel Van Lichtopsluiting, Delft University 1993 Netherlands, 1-18.
7. Itoh H. et al. Technical digest of the international PVSEC-5, Koyoto, (1990) 533-536.
8. Smith S.M. Journal of Applied physics 23(1984)2311-2326.
9. Heavens O.S. Optical properties of thin solid films, Dover publications, Inc.New York 1965.
10. Heavens O.S Thin Film physics, Methun and CO. LTD 1970, London 62-88.
11. Bohren C.F. and Huffman D.R. Absorption and Scattering of light by small particles. John wiley and sons 1983, 26-88.
12. Chopra K.L. Thin Film Phenomena, Mc. Graw Hill Book company, New York 1969, 721-793.
13. Fuhs W. Plasma deposited thin films, John wiley and sons, Chapter 3.
14. Fritzche H. Amorphous Silicon and Related Materials vol. B World Scientific Publishing Co. Pte. Ltd. 1989 U.S.A, 887-938.
15. Oriel, Andouer Corporation Optical Filters Guide
16. Oriel. Light Sources, Monochromators & Spectrographs, Detection and Detection system, Fiber Optics Vol.II.
17. Fukada, N. et al. Jpn. J.Appl. Phys. 21(1982) 271.
18. Iida, H. et al. IEEE Electron Device Letter, EDL. 4(1983)157.
19. Sato, K. et al Asahi Glass Co. Ltd Report 42(1992)129-137.

20. Kluth, O. et al Technical Digest of Miyazaki PVSEC-9 Japan 1996.
21. Schade H and Smith Z.E. Journal of Applied physics 24(1985)3221-3226.
22. Ellis. F.B. et al. MRS. Spring meeting, palo Alto, April 18,1986.
23. Forouhi A.R. EMIS Data Review RN=19027 June 1988.
24. Amensisa Abdi M.Sc. Thesis Addis Ababa University June 1995.
25. Schade H and Smith Z.E. Journal of Applied physics 57(1985)568-574.